

NASA TECHNICAL NOTE



NASA TN D-5698

0.1

NASA TN D-5698



LOAN COPY: RETURN TO
AFWL (WL0L)
KIRTLAND AFB, N MEX

EFFECT OF SURFACE PROTUBERANCES ON IMPACT LIMITERS FOR SPHERICAL HARD-LANDING PAYLOADS

by John Locke McCarty and James T. Howlett

*Langley Research Center
Langley Station, Hampton, Va.*





0132338

1. Report No. NASA TN D-5698	2. Government Accession No.	3. Recipient's Catalog No.	
4. Title and Subtitle EFFECT OF SURFACE PROTUBERANCES ON IMPACT LIMITERS FOR SPHERICAL HARD-LANDING PAYLOADS		5. Report Date March 1970	6. Performing Organization Code
		8. Performing Organization Report No. L-6886	10. Work Unit No. 124-08-29-01-23
7. Author(s) John Locke McCarty and James T. Howlett		11. Contract or Grant No.	
9. Performing Organization Name and Address NASA Langley Research Center Hampton, Va. 23365		13. Type of Report and Period Covered Technical Note	
		14. Sponsoring Agency Code	
12. Sponsoring Agency Name and Address National Aeronautics and Space Administration Washington, D.C. 20546		15. Supplementary Notes	
16. Abstract An analytical and experimental study was conducted to evaluate the effect of surface protuberances, such as rocks, on impact limiters for spherical hard-landing payloads. The analytical phase of the study consisted of the extension of an existing analysis to include protuberances and the application of this extended analysis to establish the effect of protuberances on impact-limiter design. The experimental phase of the study was undertaken to validate the analysis and consisted of impacting a realistic and full-scale (for a prospective Mars mission) hard-lander configuration, equipped with balsa as an impact limiter, onto a rigid planar surface having conical or cylindrical protuberances. The experimental results validate the capability of the extended analysis to design the impact limiter by predicting the effect of surface protuberances on limiter response.			
17. Key Words Suggested by Author(s) Hard landers Impact Impact limiters Protuberances		18. Distribution Statement Unclassified - Unlimited	
19. Security Classif. (of this report) Unclassified	20. Security Classif. (of this page) Unclassified	21. No. of Pages 42	22. Price* \$3.00

EFFECT OF SURFACE PROTUBERANCES ON IMPACT LIMITERS FOR SPHERICAL HARD-LANDING PAYLOADS

By John Locke McCarty and James T. Howlett
Langley Research Center

SUMMARY

An analytical and experimental study was conducted to evaluate the effect of surface protuberances, such as rocks, on impact limiters for spherical hard-landing payloads. The analytical phase of the study consisted of the extension of an existing analysis to include protuberances and the application of this extended analysis to establish the effect of protuberances on impact-limiter design. The experimental phase of the study was undertaken to validate the extended analysis and consisted of impacting a realistic and essentially full-scale (for a possible Mars mission) hard-lander configuration, equipped with balsa as an impact limiter, onto a rigid planar surface having cylindrical or conical protuberances. The analytical and experimental results of the study are compared on the basis of acceleration time histories and post-impact measurements which describe the impact.

The experimental results are shown to validate the capability of the extended analysis to design the impact limiter by predicting with good accuracy the effect of surface protuberances on limiter response. The data show that the analytical expressions predict the peak impact accelerations sensed by the payload and the extent of the limiter crush. Application of the analysis to limiter design indicates that limiter thickness and mass penalties are associated with an increase in either protuberance height or impact velocity.

INTRODUCTION

Hard landing of survivable scientific instruments on remote surfaces is generally considered to be a possible technique for exploring extraterrestrial bodies. One of the major problem areas associated with this technique is that of designing an impact limiter which will attenuate landing accelerations to levels acceptable to the scientific instruments. Many analytical and experimental studies have been conducted to evaluate various materials and devices suitable for impact-limiter applications. For example, references 1, 2, and 3 present the shock-alleviation characteristics of crushable foams, balsa, and honeycombs; reference 4 discusses a preliminary investigation of the

energy-absorbing potential of frangible metal tubing; references 5 and 6 review the results obtained by testing a tire-shaped hard-landing vehicle with balsa and phenolic honeycomb as impact-limiter materials; references 7, 8, and 9, respectively, present analyses of spherical configurations that employed balsa, an inflated sphere, and dove-tail phenolic honeycomb as a limiter; and references 10 and 11 offer analytical developments which treat the impact dynamics of spherical hard landers that employed a generalized crushable material as an impact limiter. These studies have concentrated upon planar impacts wherein the target was effectively a flat rigid surface. However, one significant aspect of the hard-lander approach which has received little attention is the effect of surface protuberances, such as rocks, on the design and behavior of an impact limiter. The authors know of no experimentally validated analysis which treats this effect.

The purpose of this report is to present the results of an analytical and experimental study to evaluate the effect of surface protuberances on impact limiters for spherical hard-landing payloads. The analytical phase of the study consisted of the extension of the analysis of reference 10 to include protuberances and the application of this extended analysis to establish the effect of protuberances on impact-limiter design. The experimental phase of the study was undertaken to validate the extended analysis. In this phase, bodies equipped with balsa as an impact limiter were impacted upon a rigid planar surface equipped with cylindrical or conical protuberances at a velocity realistic for a hard-landing Mars mission. The analytical and experimental results of the study are compared on the basis of acceleration time histories and post-impact measurements which describe the impact.

SYMBOLS

a_{\max}	peak acceleration
d_b	impacting body diameter
d_f	footprint diameter on target after impact
d_p	protuberance diameter
h	protuberance height
m	total mass of impacting body
t	time

t_p	time required for protuberance to penetrate impacting body
t_r	rise time to peak acceleration
V	impact velocity
δ	crush depth (maximum penetration of protuberance into impacting body)
σ_c	crushing strength of balsa parallel to grain

FACTORS INFLUENCING STUDY

At the beginning of the study, parameters were established to define the payload-limiter configuration, the target protuberances, and various impact conditions. The selected parameters were based upon a prospective hard-lander mission for exploration of the planet Mars. The chosen Mars mission defined a payload mass of 136 kg with a 3000g tolerable shock loading, a nominal impact velocity of 46 m/sec, and surface protuberances as high as 12.7 cm. Furthermore, the payload was required to survive regardless of its attitude upon impact. Although other shapes, which rely upon rather unique shock attenuation devices, have been proposed for a hard-lander configuration, it was concluded that the objectives of this study could best be achieved by using a full-scale design configuration consisting of a spherical payload encapsulated within a crushable impact-limiting material. By assuming that the density of the payload (scientific instruments, supporting equipment, and packaging structure) is 1150 kg/m³, the diameter of the payload was fixed at 61 cm.

Although other materials (plastic foams, metallic and phenolic honeycombs, for example) were considered, balsa was selected as the impact-limiter material for the present study because it has a high energy-absorbing capability per unit mass, is easy to shape, and is economical and available. Furthermore, balsa has been used for shock attenuation in some experiments (refs. 7 and 12, for example). On the basis of this experience and of calculations which considered the anticipated hard-lander sizes and impact conditions of this study, it was determined that the crushing strength of balsa would maintain impact accelerations below the tolerable 3000g level.

In view of the many types of surface protuberances, some restrictions were necessary to arrive at a reasonable program. Protuberance shapes were restricted to those which provided symmetrical impacts, that is, to those protuberances which were symmetrical about an axis coincident with the velocity vector of the impacting hard lander. Two general protuberance shapes were selected: a circular cylinder and a cone. These shapes were believed to include the extremes of symmetrical impacts. The maximum

protuberance height (distance projected beyond the planar surface) selected was 22.9 cm. This height appeared to be a reasonably severe test since only 12.7-cm protuberances were postulated for the Mars mission.

ANALYSIS

The analysis used in studying the effect of protuberances on impact limiters for hard-landing payloads is essentially that of reference 10 which has been extended to include protuberances. Details of the analysis and the related assumptions are given in the appendix. This analysis yields the time history of the motion of the impacting body from the onset of impact until the velocity of the body reaches zero. The equations describe the motion of a spherical body for three impact conditions: impact with a planar target, impact with a cylindrical protuberance on a planar target, and impact with a conical protuberance on a planar target.

APPLICATION OF ANALYSIS TO LIMITER DESIGN

The analysis was employed to determine the amount of limiter material required to protect the payload during impact with the various targets. The procedure involved the arbitrary selection of a limiter thickness, which defined the mass of the impacting body in terms of balsa density, and the computation of the response of the body during impact with a specified target. The process was repeated for different limiter thicknesses until the clearance between the payload and the target after impact was the minimum acceptable on the basis of 80 percent balsa crush-up.

The initial analytical studies of the present investigation were directed towards evaluating the effects of balsa density on the thickness of the required balsa limiter. The results of these studies indicated that, for the test conditions under consideration, the limiter thickness was essentially unaffected by the density of the balsa. A variation in balsa density from 104 to 176 kg/m³ resulted in insignificant differences in limiter thickness. The crushing strength of balsa varies directly with its density, which would imply that the higher the density, the less volume of balsa would be required to absorb a given amount of impact energy. However, for the conditions of this study, the denser limiter had a greater mass and correspondingly more impact energy to be absorbed. Thus, at least over the density range considered, the required limiter thickness remained nearly constant for all densities. Furthermore, the maximum accelerations sensed by the payload were observed to be only slightly higher for the denser limiter and were well within the 3000g constraint. Therefore, the impact limiters for the test configuration were designed analytically on the basis of a 104-kg/m³ density to yield limiters of minimum weight. (Random balsa samples examined during the fabrication process indicated

that a density of 120 kg/m^3 was more realistic.) To introduce some conservatism into the design, the impact velocity was considered to be 53 m/sec rather than 46 m/sec, the nominal test velocity.

The limiter thickness calculated to protect the 61-cm-diameter 136-kg payload during impact with a planar surface was 24 cm, which corresponded to a hard-lander sphere 109 cm in diameter. For a 22.9-cm-high protuberance, whether cylindrical or conical, the analysis defined a 170-cm-diameter hard-lander sphere.

EXPERIMENTAL APPARATUS AND TESTS

Impacting Bodies

The impacting bodies for the experimental tests consisted of a simulated payload equipped with a hemispherical shell of radial-grain balsa and sufficient ballast to equate the total mass to that of a spherical configuration. The testing technique provided the bodies with a fixed attitude at impact and thereby eliminated the need for omnidirectional protection of the test payload and thus the more formidable task of fabricating completely spherical limiters. Seven impacting bodies were fabricated: one, 109 cm in diameter, to evaluate the response during impact with a rigid flat surface in the absence of a protuberance; and six, 170 cm in diameter, to study the effects of various shape protuberances. These bodies are identified in table I, which also describes the targets and summarizes the impact test results.

In the fabrication of the bodies, steel hemispherical domes, 61 cm in diameter and 1.27 cm thick, served as the payloads to which the balsa limiters were bonded. Steps involved in the limiter fabrication are illustrated in figure 1. Balsa sections, each initially a frustum of a four-sided pyramid, were sawed from a stockpile of balsa having a nominal density of 120 kg/m^3 ($\pm 24 \text{ kg/m}^3$) so that the wood grain was radially oriented within 5° when attached to the dome. Each section was hand fitted and glued to the dome and adjacent sections as shown in figure 1(a). Once a layer of sections was completed, the assembly was mounted on a lathe and the surface of that layer was shaped with a router (fig. 1(b)) in preparation for the next layer of balsa sections. Layers were added until insufficient space was available to insert the router. A conical plug composed of several glued sections completed the balsa installation. The assembly was then returned to the lathe and the external balsa surface was cut to the desired diameter. (See figs. 1(c) and 1(d).) The balsa hemisphere was finally covered with fiber glass (figs. 1(e) and 1(f)) to act as a sealant and to minimize fragmentation during impact.

Since the analytical results showed that the crushing of balsa was limited to a spherical sector having an 80° central angle about the axis of symmetry, the requirements for complete radial-grain construction (within 5°) was relaxed in the fabrication

of bodies 2, 3, 4, and 5 to simplify and expedite the fabrication process. In the construction of these impacting bodies, the radial-grain requirement was limited to a spherical sector having a 90° central angle.

As shown in figure 2, a flange was welded to the base of each of the hemispherical steel domes to provide a means for attaching the structure required to support the impacting body on the propelling carriage. This support structure and the load-distributing aluminum plates fastened to a plywood backing sheet which was bonded to the limiter provided ballast to equate the mass of the hemispherical impacting body to the mass of a sphere of the same diameter.

Targets

The targets for the impact tests consisted of a flat rigid surface, or backstop, and the attached protuberances. The backstop was four 14 500-kg cubic blocks of reinforced concrete, with each side 1.83 m, arranged in tandem and fronted by a 1.27-cm-thick sheet of steel boilerplate which served as the target surface when no protuberance was attached. For other tests, the protuberance – a solid aluminum cylinder or cone – was affixed to the boilerplate and aligned with the axis of symmetry of the impacting body. The dimensions of the protuberance for each test are given in table I and were selected to provide targets to verify analytical trends.

Test Facility

The impact tests were performed at the Langley landing-loads track with the high-speed carriage as the propelling vehicle. A description of this facility is given in reference 13. As shown in figure 3, the impacting body was attached to the outrigger sting of the carriage and centered on a fixture within the 1.83-m-deep and 2.44-m-wide channel which parallels the track. The 58 000-kg backstop was located within the test region of the facility and centered on the floor of the channel. During operation, the impacting body was restrained within the fixture by two pins at each of the three arms of the support structure. One pin held the body in place during the carriage launching phase and was hydraulically extracted prior to impact. The other smaller pin, not extracted, was designed to contain the body on the test fixture throughout anticipated aerodynamic drag loading and was sheared upon impact of the body with the target. For the large bodies, this shearing occurred at approximately 3g. Once the pins had sheared, the body separated from the sting fixture and completed the impact while the carriage continued beyond the target to the arresting gear.

Instrumentation

Each impacting body was equipped with three piezoresistive accelerometers of different sensitivity to provide redundancy and a better definition of the impact accelerations. These accelerometers were attached to a mounting plate welded within the hemispherical dome of each body (fig. 2) and were oriented along the impact axis. Signals from each accelerometer were routed through approximately 14 m of cable, which was coiled along a carriage sting support prior to impact and terminated with a quick disconnect at a junction box on the sting. Permanent cables transmitted the acceleration signals from the junction box to a galvanometer driver amplifier and to an oscillograph recorder, all mounted on the carriage. A sample oscillograph record, which shows the response of the accelerometers during an impact, is reproduced in figure 4. Also on the record are the timing lines and signals depicting carriage displacement from which the velocity at impact was computed.

In addition to the impact acceleration time histories, high-speed motion pictures were taken from several vantage points to aid in analyzing the behavior of the bodies during impact. The sequential photographs of figure 5, for example, were extracted from the motion pictures taken by a camera adjacent to the target.

Test Procedure

The testing technique involved propelling each of the seven impacting bodies to a nominal velocity of 46 m/sec, impacting them against a planar surface equipped with a preselected protuberance, and recording the various impact characteristics. The high-speed carriage at the Langley landing-loads track was the propelling vehicle and provided impact velocities which ranged from 42.5 to 47.1 m/sec.

In preparation for a test, the protuberance was attached to the flat backstop and the impacting body was installed on the fixture of the carriage outrigger sting. The accelerometers were secured inside the hemispherical dome; and their trailing cables were coiled along a sting support and connected to the junction box. Immediately prior to launch, the onboard cameras and the recorder were started to provide a photographic and an acceleration history of events throughout the test. Other measured impact characteristics included the amount of uncrushed balsa immediately ahead of the protuberance (a distinct demarcation existed between crushed and uncrushed balsa) and the diameter of the footprint left by the impacting body on the target surface.

PRESENTATION OF DATA

Acceleration data describing each impact test were obtained from an oscillograph record of the outputs of the three accelerometers. The accelerometer responses are

typified by the sample record of figure 4 in which signals from the accelerometers are reproduced. Fairing of the acceleration signals was required to ascertain the impact response since the signals contained a high-frequency response which was found to correspond to a natural frequency of the steel hemispherical dome. To arrive at a single impact acceleration time history for each test, the outputs from the three accelerometers were faired independently and compared. The reported acceleration time history is the mean of the outputs from the accelerometers of lower sensitivity, which are less influenced by the high-frequency noise. The experimental acceleration time histories were faired with a sharp discontinuity following the peak acceleration because of the difficulty in distinguishing the exact shape of the time history at that point. These faired experimental acceleration time histories and the corresponding acceleration time histories developed analytically are presented in figure 6. Two analytical acceleration time histories are given for each test, one for each of two different values of balsa crushing strength σ_c . The values of σ_c were taken from reference 1 which lists average mean crushing strengths for various ranges of balsa density. The density of the balsa used in the fabrication of the impacting bodies varied within two of these ranges; hence, two sets of analytical results were obtained: one based upon $\sigma_c = 8500 \text{ kN/m}^2$ from the lower density range and one using $\sigma_c = 10\,000 \text{ kN/m}^2$ from the higher density range. Other parameters necessary to obtain the analytical results (impacting body mass and diameter, impact velocity, etc.) correspond to the experimental values for each individual test.

Pertinent characteristics of the experimental and analytical acceleration time histories for all impact tests and other significant impact features are summarized in table I. Characteristics of the acceleration time histories consist of the peak acceleration a_{max} ; the rise time to reach the peak acceleration t_r , measured from onset of impact; and the time required for the protuberance to penetrate the impacting body t_p , also measured from onset of impact.

Other impact characteristics listed in the table are the crush depth δ and the footprint diameter d_f . The crush depth is defined as the maximum penetration of the protuberance into the balsa limiter (for impact on a flat surface, it is the maximum penetration of the plane target surface) and is determined experimentally by measuring the uncrushed balsa which remains between the protuberance and the payload and by assuming that balsa crushes to 20 percent of its original length. Footprint diameter is defined as the diameter of the circular pattern left on the backstop after the impact. Trends which indicate the effects of protuberance size and shape on some of these impact characteristics are presented in figures 7, 8, and 9. Figures 10, 11, and 12 present the results of analytical studies to describe the effects of variations in parameters associated with the design of a limiter for a hard-landing payload.

DISCUSSION OF RESULTS

Impact Behavior

The physical behavior of the bodies during impact was studied visually from high-speed motion pictures. The cylindrical protuberances cleanly sheared the limiter around the periphery of the protuberance and punched a cylinder of crushed balsa immediately ahead of the face of the protuberance. Similarly, the conical protuberances induced a crushing failure in the balsa with no apparent tendency to fracture the limiter. As shown in figure 5, the spherical nose body impinging the flat planar surface appeared to produce pure crushing in the limiter fibers over an area described by the plane of contact between the body and the surface.

In all impact tests, the impact limiter split into usually three, or sometimes four, sections and separated from the simulated payload. However, motion pictures of the impacts revealed that the cracks in all limiters except that of body 3 developed in the limiter after maximum penetration had been reached (body velocity reduced to zero); these cracks originated at the rear of the hemispherical limiter and propagated forward. An inspection after the tests revealed that these cracks occurred along apparent shear planes and not along the glued joints. The splitting was attributed to the unique mounting technique (three-arm support structure) employed in these tests, and it is believed that the impact limiter for a completely spherical hard lander would remain intact. Since the splitting did not occur until after the impacting bodies had come to rest against the target, the recorded acceleration time histories were not affected to at least maximum acceleration.

The behavior of the impacting bodies for which the radial-grain requirement (within 50°) was limited to only those areas involved during impact did not appear to differ from that of the bodies fabricated entirely from radial-grain balsa. This similarity implies that for unidirectional (controlled attitude) impact testing of balsa limiters, the fabrication process can be greatly simplified by adhering to the radial-grain requirement only in the zone influenced by the impact.

Acceleration time histories.- The faired acceleration time history for each of the impact tests and the corresponding analytically developed acceleration time histories based upon two values of balsa crushing strength are presented in figure 6. In the analytical treatment, the impacts are considered to be plastic; thus, the analytical time histories cease when the velocity of the impacting body reaches zero. In contrast, the experimental time histories continue until the acceleration reaches zero and include the restitution (rebound) which was observed. The overall agreement between the experimental and the analytical acceleration time histories is considered good, particularly in view of the possible variations in physical properties of the individual balsa segments from which the

limiters were fabricated. In general, the analytical acceleration time histories described by the lower value of balsa crushing strength, $\sigma_c = 8500 \text{ kN/m}^2$, better define the experimental time histories.

The primary difference in the shapes of the analytical and experimental time histories is in the slope of the increasing accelerations following contact of the body with the planar surface. However, refinement of the expression which relates the variation in balsa crushing strength to grain angle (eq. (A1)) may result in better correlation. Some difference may also be noted in the shape of the time histories during penetration of the cylindrical protuberance. The analysis assumes that all crushing occurs at the face of the protuberance, whereas it was observed from the tests that a significant amount of crushing occurred near the hemispherical dome (payload) ahead of the protuberance. Apparently crushing occurs adjacent to the payload because the punched cylinder of balsa ahead of the protuberance is weakest in this region due to the grain-angle effect.

In the acceleration time history for body 3 (fig. 6(c)), a pronounced drop in the experimental acceleration commences at approximately 5 msec. This drop is attributed to splitting of the impact limiter during penetration of the protuberance as observed from the films. The slight rise near the end of the analytical acceleration time history for $\sigma_c = 8500 \text{ kN/m}^2$ results from impact of the body with the planar surface.

General characteristics.- Characteristics of the acceleration time histories of figure 6 (summarized in table I) indicate generally good agreement between experiment and analysis. The maximum acceleration observed, either experimentally or analytically, throughout this study was less than 1300g, well below the tolerable limit of 3000g.

Except for the impact test of body 3, the analysis predicts with reasonable accuracy the experimental rise times. The apparent discrepancy in t_r associated with body 3 is attributed to the unique shape of the acceleration time history (fig. 6(c)) for a 55.9-cm protuberance diameter. As discussed subsequently in the section entitled "Effect of Protuberance Geometry on Impact Characteristics," the analysis shows a discontinuous jump in t_r from 12 msec down to 1 msec at approximately this diameter. (See fig. 7.)

The time required for the protuberance to penetrate the limiter t_p can be determined with reasonable accuracy from the shape of the experimental acceleration time histories, whereas analytically that time is precise due to the mathematical discontinuity. Some of the minor differences between the experimental and analytical values of t_p can be attributed to the crushing behavior of the balsa ahead of the protuberance.

The crushing behavior of the balsa may also at least partially explain the minor differences (table I) between analytical and experimental crush depths. It should be pointed out that in all impact tests, the crush depth never exceeded the amount available; some uncrushed balsa always remained between the protuberance and the payload. Thus,

at a nominal impact velocity of 46 m/sec, 24 cm of balsa (19.2 cm available crush depth) was sufficient to protect the payload during a planar impact, whereas a limiter thickness of 54.5 cm (43.6 cm available crush depth) was required to protect the payload from a 22.9-cm-high protuberance. Hence, it may be concluded that the limiter design for body 1 was satisfactory for impact on a flat surface and the limiter design for the other bodies was satisfactory for impacts on the 22.9-cm-high protuberances.

The experimental footprint diameter for body 1 (no protuberance) is in excellent agreement with that predicted analytically by using the lower crushing strength for balsa. For the bodies impacting the various protuberances, the experimental footprints are consistently larger than those calculated. However, the size of the footprints indicates that crushing in all of the bodies occurred within a spherical sector having a 90° cone angle. The experimental data confirm the relative invariance in footprint diameter as predicted for the various protuberances.

Effect of Protuberance Geometry on Impact Characteristics

In order to evaluate the effect of protuberances on the impact characteristics of hard-lander designs, the analysis was used to obtain trends of the impact characteristics associated with variations in the protuberances. Input parameters for the analysis were based upon mean values of the impact velocity and mass of appropriate test bodies to permit a comparison with the experimental results. The crushing strength of the balsa impact limiters for these bodies was considered to be 8500 kN/m^2 . Impact characteristics chosen to illustrate the trends were the peak impact acceleration a_{max} , the rise time to peak acceleration t_r , and the maximum crush depth δ . The effects on the characteristics attributed to the diameter and height of cylindrical protuberances and to the total included angle of conical protuberances are examined separately.

Diameter of cylindrical protuberance.- Figure 7 shows the variation of the computed significant impact characteristics with the diameter of the 22.9-cm-high cylindrical protuberances. Results from related tests are also included in the figure and are shown to verify the analytical trends. The peak acceleration a_{max} decreases with an increase in d_p until a minimum value is reached at $d_p \approx 56 \text{ cm}$ (corresponding to 33 percent d_b) and then increases for larger values of d_p . At protuberance diameters below 56 cm, the entire protuberance penetrates the limiter and the maximum acceleration occurs when the body impacts the planar surface. For smaller protuberances, less energy is removed from the impacting body, which results in greater accelerations during impact with the plane. As the protuberance diameter increases beyond 56 cm, less of the protuberance penetrates the body and the protuberance begins to resemble a planar surface. Calculations show that the maximum acceleration increases in this region ($d_p > 56 \text{ cm}$) until the protuberance diameter is approximately 65 percent of the impacting body diameter

(170 cm); for larger protuberance diameters, the maximum acceleration is identical to that for a planar surface. When the protuberance gives the appearance of a plane, the maximum acceleration occurs during impact of the body with the face of the protuberance and not with the backstop surface to which the protuberance is mounted. This transition produces a discontinuity in the rise time to peak acceleration t_r , as illustrated by the variation of t_r with d_p .

For impacts in which the protuberance does not resemble a planar surface, the penetration, and hence the crush depth, is a function of the amount of impact energy absorbed during penetration of the protuberance. Thus, as the diameter of the protuberance increases (fig. 7), the limiter crush depth decreases to a value corresponding to that for impact with a planar surface. The difference between the crush depths of very small and very large diameter protuberances is equal to the protuberance height. The maximum available crush depth denoted in the figure corresponds to the 80-percent allowable crush depth assumed for balsa and is shown to provide the body design with an approximately 4-cm clearance.

Height of cylindrical protuberance.- Figure 8 presents the effect of protuberance height on the significant impact characteristics for a 38.1-cm-diameter cylindrical protuberance. The analytical and related experimental data are based upon an impacting body design for a 22.9-cm-high protuberance, which accounts for the considerable clearance in available crush depth at the low protuberance heights. The figure shows that the trends described by the impact characteristics developed analytically are corroborated by data from the two related experimental tests.

As discussed previously, a protuberance with a diameter of 38.1 cm penetrates the impact limiter (does not act as a planar surface) and the maximum acceleration occurs when the body impacts the flat backstop. Thus, as the height of the protuberance is increased over the range considered (fig. 8), the maximum acceleration decreases since the impact energy absorbed by the protuberance increases with protuberance height. Furthermore, the rise time to maximum acceleration increases with the increase in height of the protuberance since the body requires more time, from onset of impact, to impact the backstop.

Included angle of conical protuberance.- Figure 9 presents variations of the significant impact characteristics with the included angle of a 22.9-cm-high conical protuberance. Since the experimental data for cone angles of 40° and 100° were acquired at two slightly different impact velocities, two sets of analytical results are presented - one for each test impact velocity - to permit a direct comparison with the experimental results. As the cone angle increases from near zero to 180° , the maximum acceleration decreases only slightly up to an angle of approximately 100° , decreases pronouncedly to a minimum at a cone angle of approximately 120° , and then increases as the

protuberance begins to resemble a planar surface. The maximum acceleration decreases with an increase in cone angles to approximately 120° because the larger conical protuberances absorb more of the impact energy. The acceleration for impacts on a 180° cone is analytically identical to that for impacts on cone angles approaching 0° , since both protuberances are essentially planar surfaces. However, the rise time and the crush depth for near-zero and 180° cone angles differ. As the shape of the cone approaches a flat plate, penetration of the protuberance into the limiter decreases until at a cone angle of 180° the crush depth is exactly 22.9 cm (protuberance height) less than that at very small cone angles. Similarly, the time to peak acceleration decreases at the higher cone angles because of the decreased penetration. For cone angles less than approximately 100° , the rise time and the crush depth, like the peak acceleration, are essentially constant.

The analytical results of figure 9 also show that an increase in the impact velocity produces an increase in maximum acceleration and crush depth and a slight decrease in rise time. From the standpoint of limiter design, the critical characteristic is the crush depth since at low conical angles the limiter provides only a minimal clearance.

Analytically Determined Influence of Protuberances on Limiter Design

Having been shown to be capable of predicting with reasonable accuracy the response behavior of a hard-landing configuration during impact with specified protuberances, the analytical technique was used to study the interdependent effects of protuberance height, limiter thickness, and impact velocity on limiter design.

Impact body design guidelines.- The trends shown in figures 7, 8, and 9 indicate that the most severe protuberance in terms of peak acceleration and crush depth is one having a small cross-sectional area, regardless of shape. Thus, to provide a severe impact condition, the protuberance selected for this phase of the study was a 2.54-cm-diameter cylinder. Furthermore, the data in figures 7 and 9 indicate that the impact response from this protuberance would also apply to conical protuberances with cone angles less than 100° . For the limiter design phase of the analysis, the assumptions were made that the payload is a 61-cm-diameter sphere with a mass of 136 kg and that the impact limiter is balsa having a density of 104 kg/m^3 and a crushing strength parallel to the grain of 8500 kN/m^2 .

Effect of protuberance height.- Figure 10 presents the thickness of a balsa limiter required to protect the payload during impact at a velocity of 45.7 m/sec with protuberances ranging in height up to 45 cm. The corresponding mass of the limiter is also presented to illustrate the mass penalty for protection against protuberances. Similar curves can be derived from the analysis for other velocities, payloads, and limiter materials. At limiter thicknesses less than those described by the curve, the balsa "bottoms

out" and in effect the payload strikes a rigid target, which results in greatly increased accelerations and possible damage to the payload structure. The figure shows that the design of limiters for protuberances does not entail the simple addition of limiter thickness equal to the protuberance height to the limiter for a planar impact. For example, at a protuberance height of 30 cm, the required limiter thickness for the conditions considered is about 59 cm, which is approximately 9 cm greater than the combined thickness for no protuberance (20 cm) and the protuberance height. Additional limiter thickness is necessary to provide for the increase in kinetic energy of the impacting body of larger body mass.

Effect of impact velocity.- In figure 11 the amount of limiter material (thickness and mass) required to protect the payload is presented as a function of the velocity at impact with a protuberance of fixed height. The curves of this figure relate to an arbitrarily selected protuberance height of 25 cm; however, similar curves can be developed from the analysis for other heights as well as other payloads and limiter materials. The figure shows the importance of impact velocity considerations in the design of a limiter for a particular protuberance height. The greater the impact velocity, the more limiter material is required to absorb the increased energy of the impacting system. A spherical hard-landing payload, which requires omnidirectional protection, such as the one under consideration, is seen to suffer a severe mass penalty, particularly at the higher impact velocities, since the additional limiter thickness must be applied over the entire spherical surface.

Protection for off-design conditions.- Figure 12 shows the effect of protuberance height on the allowable impact velocity for a fixed-configuration design. To illustrate this effect, a body was designed on the basis of the limiter required to protect the payload during impact at 45.7 m/sec on a 25-cm-high protuberance. At these impact conditions, the analysis defined a balsa limiter which was 51.75 cm thick and had a mass of 231 kg. This limiter design corresponds to points on the curves of both figures 10 and 11 for the appropriate impact conditions. The curve of figure 12 was obtained by computing the maximum impact velocity for which the limiter of the design configuration affords protection to the payload against protuberances ranging up to 40 cm in height. Thus, in effect, any point on this curve would design the same hard-lander configuration. For combinations of impact conditions (velocity and protuberance height) which fall below the curve, the payload is provided with ample protection; for those combinations which fall above, insufficient limiter is available and the payload bottoms out and in effect impacts a rigid target.

As expected, the figure shows that for protuberances higher than that for which the hard lander is designed, the impact velocity must be reduced for the payload to survive. Similarly, if the impact velocity is higher than the design velocity, the limiter will only

provide adequate protection for protuberances shorter than those for which the configuration was designed. It would appear that in a hard-lander application, curves similar to that of figure 12 would be useful in assessing the probability of a successful landing on a surface of unknown protuberance sizes for missions in which some control over the impact velocity is provided.

CONCLUDING REMARKS

An analytical and experimental study was made to evaluate the effect of surface protuberances on impact limiters for spherical hard-landing payloads. In the experimental phase of the study, tests were performed with a hard-lander configuration, equipped with a balsa impact limiter, which impacted at a nominal velocity of 46 m/sec a rigid planar surface having cylindrical or conical protuberances. The following remarks are based upon a comparison of these experimental results with results obtained from an existing analysis for planar impacts which was extended to include protuberances.

In general, the experimental results demonstrate the capability of the analysis to predict the behavior of hard-landing payloads impacting on various protuberances. Acceleration time histories recorded during the experiments compare favorably with those generated analytically. In particular, significant features of these time histories, such as peak acceleration and characteristic times, are in agreement. Other impact characteristics, which consist of the extent of limiter crush and the size of the footprint on the target surface, are predicted with acceptable accuracy. The effect of protuberance geometry on impact characteristics indicates that protuberance shape and cross section have little effect until the protuberance begins to resemble a planar surface. The application of the analysis to limiter design indicates that limiter thickness and mass penalties are associated with an increase in either protuberance height or impact velocity.

Langley Research Center,

National Aeronautics and Space Administration,

Langley Station, Hampton, Va., December 16, 1969.

APPENDIX

ANALYSIS

This appendix develops the equations of motion which describe the impact of a spherical body, consisting of a payload encapsulated within a crushable balsa limiter, with the rigid targets of the present study. These equations are essentially those of reference 10, which treats only rigid planar targets, extended to include protuberances. The assumptions used in the development are as follows:

1. Variations in the mass undergoing deceleration due to the crushing of the balsa are neglected. This assumption has been evaluated (ref. 10, for example) and found to be valid at impact velocities less than 76.2 m/sec.

2. The impact occurs in a zero-gravity environment. The weight of the impacting system is negligible relative to the force exerted on the system by the crushing balsa. This assumption is exact with respect to the tests of the present study since the impacts were performed horizontally.

3. The effects attributed to shock waves generated in the balsa during impact are neglected. In reference 7, these effects are shown to be small for spherical impact limiters with radially oriented grain at impact velocities less than 137 m/sec.

4. The balsa crushes in a plane which coincides with the impact surface; thus, the effects of built-up layers of crushed balsa ahead of the impact surface are neglected. This assumption is a first approximation since the shape of the surface of the crushed layer of balsa and its effects are not clearly understood.

5. The balsa limiter is of uniform density and has radially oriented grain.

6. Balsa crushes to 20 percent of its original length. This commonly used assumption determines the minimum acceptable clearance between the payload and the protuberance at the conclusion of the impact. (For example, see ref. 7.)

7. The variation of balsa crushing strength σ with grain angle θ is given by the relationship

$$\sigma(\theta) = \sigma_c \left(1 - \frac{2.7}{\pi} \theta \right) \quad (A1)$$

where σ_c is the crushing strength of the balsa parallel to the grain and is assumed to remain constant during crush. The limited available data, including the results of some tests made in conjunction with this study, do not clearly establish the exact form of $\sigma(\theta)$; however, equation (A1) appears to be a reasonable first approximation for values of θ up to $\pi/3$, which is sufficient for the present application.

APPENDIX

Planar Target

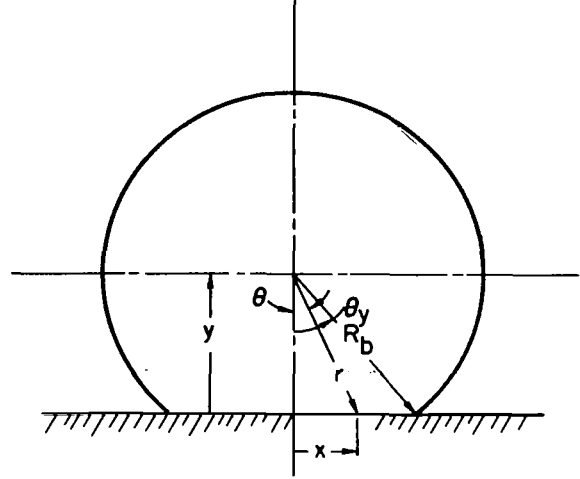
The impact of a spherical body on a rigid planar surface is represented by the system given in sketch 1. The equation of motion for this system is of the form

$$m\ddot{y} = F(y)$$

where m is the total mass of the impacting system, y is the distance from the planar surface to the center of gravity of the spherical body, and $F(y)$ is the force exerted on the system. The force $F(y)$ which results from the crushing of balsa at the impact plane, is obtained by integrating σ over the surface of contact between the plane and the sphere, or

$$F(y) = \int_0^{\theta_y} dF = \int_0^{\theta_y} \sigma(\theta) dA$$

where θ_y , as shown in sketch 1, is the angle which describes the contact region.



Sketch 1

For an incremental area dA of an annular strip of width dx at a distance x from the impact center line,

$$dA = 2\pi x dx$$

From sketch 1, $x = y \tan \theta$; hence,

$$dA = 2\pi y^2 \frac{\tan \theta}{\cos^2 \theta} d\theta$$

With this equation and the relationship

$$\theta_y = \cos^{-1} \frac{y}{R_b}$$

where R_b is the radius of the spherical impacting body, the expression for the force becomes

$$F(y) = \int_0^{\cos^{-1} \frac{y}{R_b}} 2\pi \sigma(\theta) y^2 \frac{\tan \theta}{\cos^2 \theta} d\theta \quad (A2)$$

Substituting equation (A1) into equation (A2) and integrating leads to the following equation of motion:

$$m\ddot{y} = \sigma_c \pi \left[R_b^2 - y^2 - \frac{2.7}{\pi} \left(R_b^2 \cos^{-1} \frac{y}{R_b} - y \sqrt{R_b^2 - y^2} \right) \right] \quad (A3)$$

APPENDIX

Equation (A3) was numerically integrated by the Runge-Kutta method for impacts involving a planar target surface. The integration was stopped when the velocity of the impacting sphere reached zero (i.e., when \dot{y} changed sign).

Cylindrical Protuberance on a Planar Target

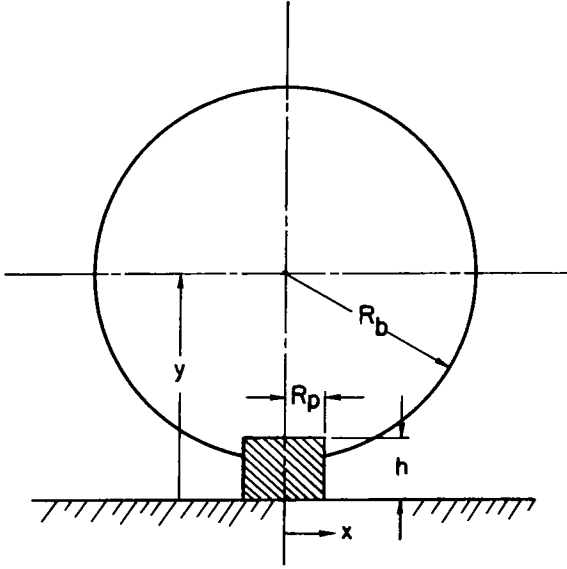
For impacts on a cylindrical protuberance, the axis of the cylinder is considered to be normal to the surface plane and centered on the impacting sphere. The geometry and notation for such an impact are shown in sketch 2. During the initial phase of the impact, when

$$R_b^2 \leq (y - h)^2 + R_p^2$$

(where h and R_p are the protuberance height and radius, respectively), the sphere is in contact with only the face of the cylinder and the equation of motion is the same as equation (A3) with y replaced by $y - h$. When

$$(y - h)^2 + R_p^2 < R_b^2 \leq y^2 + R_p^2$$

which corresponds to the configuration shown in the sketch, the force equation (A2) becomes



Sketch 2

$$F(y) = \int_0^{\cos^{-1} \frac{y-h}{\sqrt{(y-h)^2 + R_p^2}}} 2\pi\alpha(\theta)(y - h)^2 \frac{\tan \theta}{\cos^2 \theta} d\theta \quad (A4)$$

Substituting equation (A1) into equation (A4) and integrating leads to the following equation of motion which describes the second phase of the impact:

$$m\ddot{y} = \sigma_c \pi \left(R_p^2 - \frac{2.7}{\pi} \left\{ \left[R_p^2 + (y - h)^2 \right] \cos^{-1} \frac{y - h}{\sqrt{R_p^2 + (y - h)^2}} - (y - h)R_p \right\} \right) \quad (A5)$$

The final phase of the impact ($R_b^2 > y^2 + R_p^2$) commences when the sphere contacts the planar backstop surface and the force equation is equation (A4) with an additional term to account for this planar impact. The additional term is

APPENDIX

$$\int_{\tan^{-1} \frac{R_p}{y}}^{\cos^{-1} \frac{y}{R_b}} 2\pi\sigma(\theta)y^2 \frac{\tan \theta}{\cos^2 \theta} d\theta$$

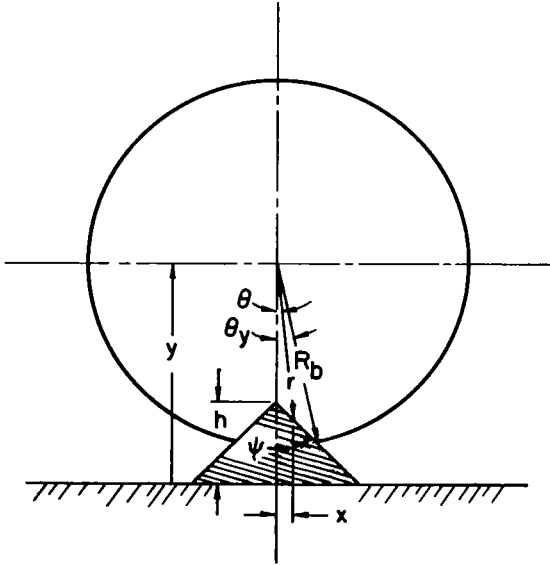
Hence, the equation of motion for this phase is

$$m\ddot{y} = \sigma_c \pi \left(R_p^2 - \frac{2.7}{\pi} \left\{ \left[R_p^2 + (y-h)^2 \right] \cos^{-1} \frac{y-h}{\sqrt{R_p^2 + (y-h)^2}} + hR_p \right\} + R_b^2 - (y^2 + R_p^2) - \frac{2.7}{\pi} \left[R_b^2 \cos^{-1} \frac{y}{R_b} - (R_p^2 + y^2) \tan^{-1} \frac{R_p}{y} - y \sqrt{R_b^2 - y^2} \right] \right) \quad (A6)$$

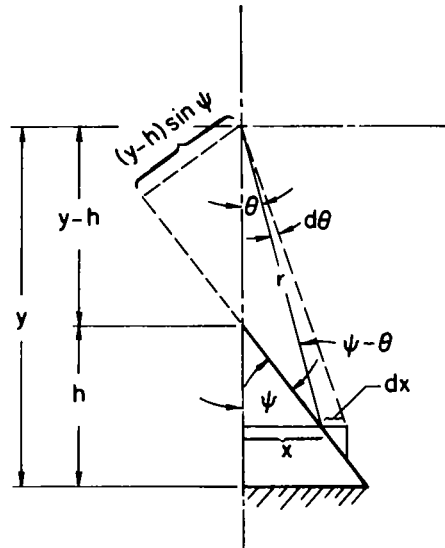
Equations (A5) and (A6) were solved by the Runge-Kutta numerical integration method.

Conical Protuberance on a Planar Target

The geometry and notation used to describe the impact of a sphere on a cone protruding from a planar surface are shown in sketches 3 and 4. Again, only a symmetrical



Sketch 3



Sketch 4

normal impact is considered, and all limiter crushing is assumed to occur parallel to the direction of impact. Sketch 4 shows that as θ increases by an amount $d\theta$, the projection of the included conical surface area perpendicular to the path of the sphere is an annular strip of width dx and area

$$dA = 2\pi x dx$$

APPENDIX

The incremental force exerted on the system by the cone is approximated by

$$dF = \sigma(\theta) dA$$

and hence

$$F(y) = \int_0^{\theta_y} 2\pi\sigma(\theta) x dx$$

With the use of equation (A1) and the relationships

$$x = \frac{(y - h)\sin \psi \sin \theta}{\sin(\psi - \theta)} \quad (A7)$$

and

$$\theta_y = \psi - \sin^{-1} \frac{(y - h)\sin \psi}{R_b}$$

where ψ is the included cone half-angle, the following equation of motion was developed which is valid during impact until the sphere contacts the planar surface:

$$\begin{aligned} m\ddot{y} = & 2\pi\sigma_c \sin^2 \psi \left(\frac{1}{2} R_b^2 + \left(\cos^2 \psi - \frac{1}{2} \right) (y - h)^2 - (y - h) \cos \psi \sqrt{R_b^2 - (y - h)^2 \sin^2 \psi} \right. \\ & - \frac{2.7}{\pi} \left\{ \left[\psi - \sin^{-1} \frac{(y - h)\sin \psi}{R_b} \right] \left[\frac{R_b^2}{2} - (y - h) \cos \psi \sqrt{R_b^2 - (y - h)^2 \sin^2 \psi} \right] \right. \\ & \left. \left. - \frac{1}{2} (y - h) \sin \psi \sqrt{R_b^2 - (y - h)^2 \sin^2 \psi} + (y - h)^2 \sin \psi \cos \psi \left(\frac{1}{2} + \log_e \frac{R_b}{y - h} \right) \right\} \right) \quad (A8) \end{aligned}$$

when the sphere impacts the planar surface, the force is

$$F(y) = \int_0^{\tan^{-1} \frac{h \tan \psi}{y}} 2\pi\sigma(\theta) x dx + \int_{\tan^{-1} \frac{h \tan \psi}{y}}^{\cos^{-1} \frac{y}{R_b}} 2\pi\sigma(\theta) x dx$$

where x is given by equation (A7) for the first integral and by $x = y \tan \theta$ for the second integral. The equation of motion for this phase of the conical impact is

APPENDIX

$$\begin{aligned}
 m\ddot{y} = 2\pi\sigma_c \left[\sin^2\psi \left(\frac{1}{2}(h^2\tan^2\psi + y^2) + \left(\cos^2\psi - \frac{1}{2}\right)(y-h)^2 - (y-h)\cos\psi\sqrt{h^2\tan^2\psi + y^2 - (y-h)^2\sin^2\psi} \right. \right. \\
 - \frac{2.7}{\pi} \left\{ \left[\psi - \sin^{-1} \frac{(y-h)\sin\psi}{\sqrt{h^2\tan^2\psi + y^2}} \right] \left[\frac{h^2\tan^2\psi + y^2}{2} - (y-h)\cos\psi\sqrt{h^2\tan^2\psi + y^2 - (y-h)^2\sin^2\psi} \right] \right. \\
 \left. \left. - \frac{1}{2}(y-h)\sin\psi\sqrt{h^2\tan^2\psi + y^2 - (y-h)^2\sin^2\psi} + (y-h)^2\sin\psi\cos\psi \left(\frac{1}{2} + \log_e \frac{\sqrt{h^2\tan^2\psi + y^2}}{y-h} \right) \right\} \right] \\
 + \frac{R_b^2}{2} - \frac{1}{2}(y^2 + h^2\tan^2\psi) - \frac{2.7}{\pi} \left[\frac{R_b^2}{2} \cos^{-1} \frac{y}{R_b} - \frac{1}{2}(y^2 + h^2\tan^2\psi) \tan^{-1} \frac{h\tan\psi}{y} \right. \\
 \left. - \frac{1}{2}y\sqrt{R_b^2 - y^2} + \frac{1}{2}yh\tan\psi \right] \quad (A9)
 \end{aligned}$$

Equations (A8) and (A9) were also numerically integrated by the Runge-Kutta method.

REFERENCES

1. Daigle, D. L.; and Lonborg, J. O.: Evaluation of Certain Crushable Materials. Tech. Rep. No. 32-120 (Contract No. NASw-6), Jet Propulsion Lab., California, Inst. Technol., Jan. 13, 1961.
2. Anon.: RF Transparent, Energy Absorbing, Structural Elements - Phase II. Doc. No. 64SD4329 (JPL Contract No. 950564), Missile and Space Div., Gen. Elec. Co., Aug. 17, 1964.
3. Conn, Andrew F.: Impact Energy Absorption Properties of Crushable Materials. RM-315, Martin Co., Oct. 1966.
4. McGehee, John R.: A Preliminary Experimental Investigation of an Energy-Absorption Process Employing Frangible Metal Tubing. NASA TN D-1477, 1962.
5. Meyers, Wm. M.: Development of Energy-Dissipating Plastic Honeycomb. Doc. No. 68SD4264 (JPL Contract No. 951172), Missile and Space Div., Gen. Elec. Co., June 14, 1968.
6. Knoell, A. C.: Structural Development of an Impact Limiter System for a Mars Landing Vehicle. AIAA Paper No. 68-961, Sept. 1968.
7. Anon.: Impact Technology Document. Publ. No. U-3031 (JPL Contract No. 950996), Aeronutronic, Feb. 25, 1965.
Vol. I - Introduction and Analysis.
Vol. II - Balsa Wood and Mechanical.
8. Ross, R. G., Jr.; and Layman, W. E.: The Design and Testing of an Inflated Sphere Impact Limiter. Tech. Rep. No. 32-1037 (Contract No. NAS 7-100), Jet Propulsion Lab., California Inst. Technol., Dec. 15, 1966.
9. Knoell, A. C.: Analysis of the Crushing of a Dovetail Phenolic Honeycomb Spherical Impact Limiter. Tech. Rep. No. 32-1287 (Contract No. NAS 7-100), Jet Propulsion Lab., California Inst. Technol., July 1, 1968.
10. Cloutier, Gerald J.: Landing Impact Energy Absorption Using Anisotropic Crushable Materials. J. Spacecraft, vol. 3, no. 12, Dec. 1966, pp. 1755-1761.
11. Berkowitz, Harvey M.; and Rodriguez, David A.: Dynamic Analysis and Development of Response Histories and Tradeoff Study Charts for Spherical Impact Limiters. J. Spacecraft, vol. 6, no. 1, Jan. 1969, pp. 50-58.
12. McCarty, John Locke; and Carden, Huey D.: Response Characteristics of Impacting Penetrometers Appropriate to Lunar and Planetary Missions. NASA TN D-4454, 1968.

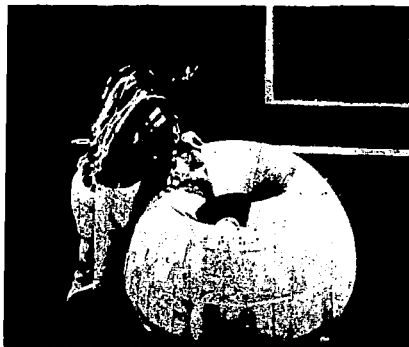
13. Joyner, Upshur T.; Horne, Walter B.; and Leland, Trafford J. W.: Investigations on the Ground Performance of Aircraft Relating to Wet Runway Braking and Slush Drag. AGARD Rep. 429, Jan. 1963.

TABLE I.- TEST CONDITIONS AND SUMMARY OF IMPACT RESULTS

Impact body			V, m/sec	Target (dimensions in cm)	Impact results									
					a_{max} g units		t_r , msec		t_p , msec		δ , cm		d_f , cm	
Designation	d_b , cm	m, kg			Exp.	Anal. (a)	Exp.	Anal. (a)	Exp.	Anal. (a)	Exp.	Anal. (a)	Exp.	Anal. (a)
1	109	191	46.2		1230	1230 1075	5.2	5.2 5.7	---	---	11.4	14.2 15.7	76.2	73.4 76.7
2	170	414	47.1		1100	1125 1015	9.1	7.2 7.8	1.8	2.2 2.1	23.4	22.2 23.9	112	95.2 100.4
3	170	416	44.5		420	483 410	^b 4.5	1.1 1.1	---	---	30.5	23.6 27.7	---	---
4	170	421	45.7		750	890 850	12	11.2 11.6	5.4	6.4 6.2	39.6	33.7 35.6	107	82.6 89.4
5	170	420	43.2		1250	1090 990	11.6	10.9 11.5	4.8	5.5 5.4	37.6	37.1 38.5	109	94.8 98.4
6	170	424	42.5		950	1080 975	10.2	11.0 11.6	5.0	5.5 5.5	33	37.1 38.5	105	94.0 98.3
7	170	423	46.6		950	1015 935	12.6	10.6 11.2	6.6	6.3 6.2	39.6	35.8 37.6	109	90.2 95.8

^aUpper value based on $\sigma_c = 10\ 000\ \text{kN/m}^2$; lower value based on $\sigma_c = 8500\ \text{kN/m}^2$.

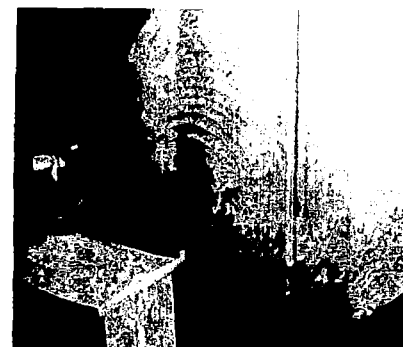
^bSee figure 6(c).



(a) Hand fitting balsa sections to hemispherical dome.



(b) Shaping surface of a balsa layer.



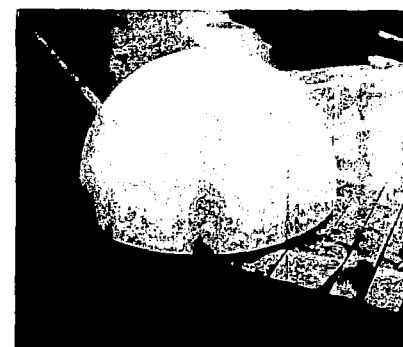
(c) Preliminary cut of external surface.



(d) Final cut of external surface.



(e) Application of fiber glass.



(f) Completed body.

Figure 1.- Steps involved in fabrication of impact limiters for hard-lander tests. Body 1.

L-69-4281

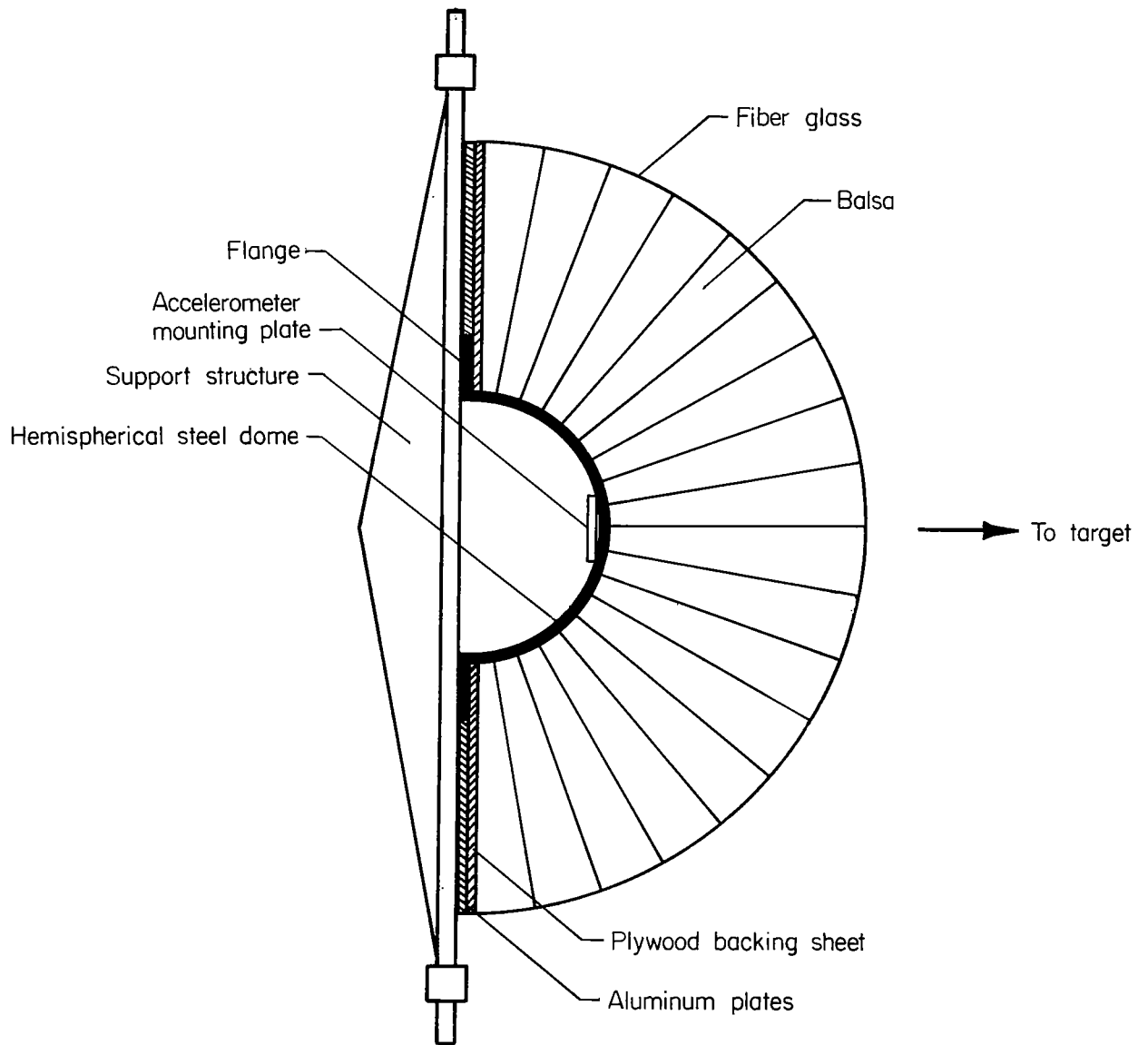


Figure 2.- Top cross-sectional view showing construction details of impact body.

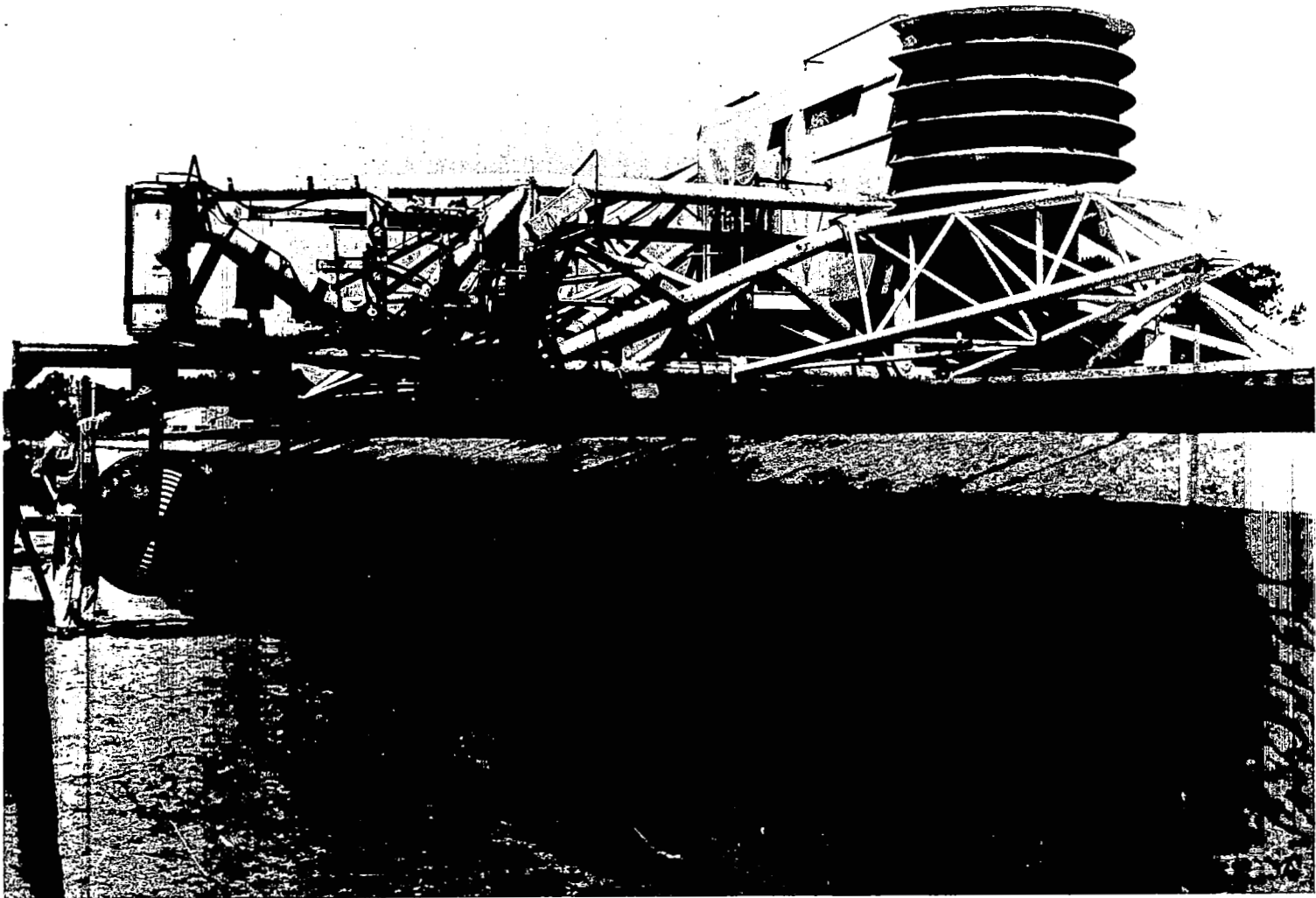


Figure 3.- Impact body 1 on sting of high-speed carriage at Langley landing-loads track.

L-69-3407

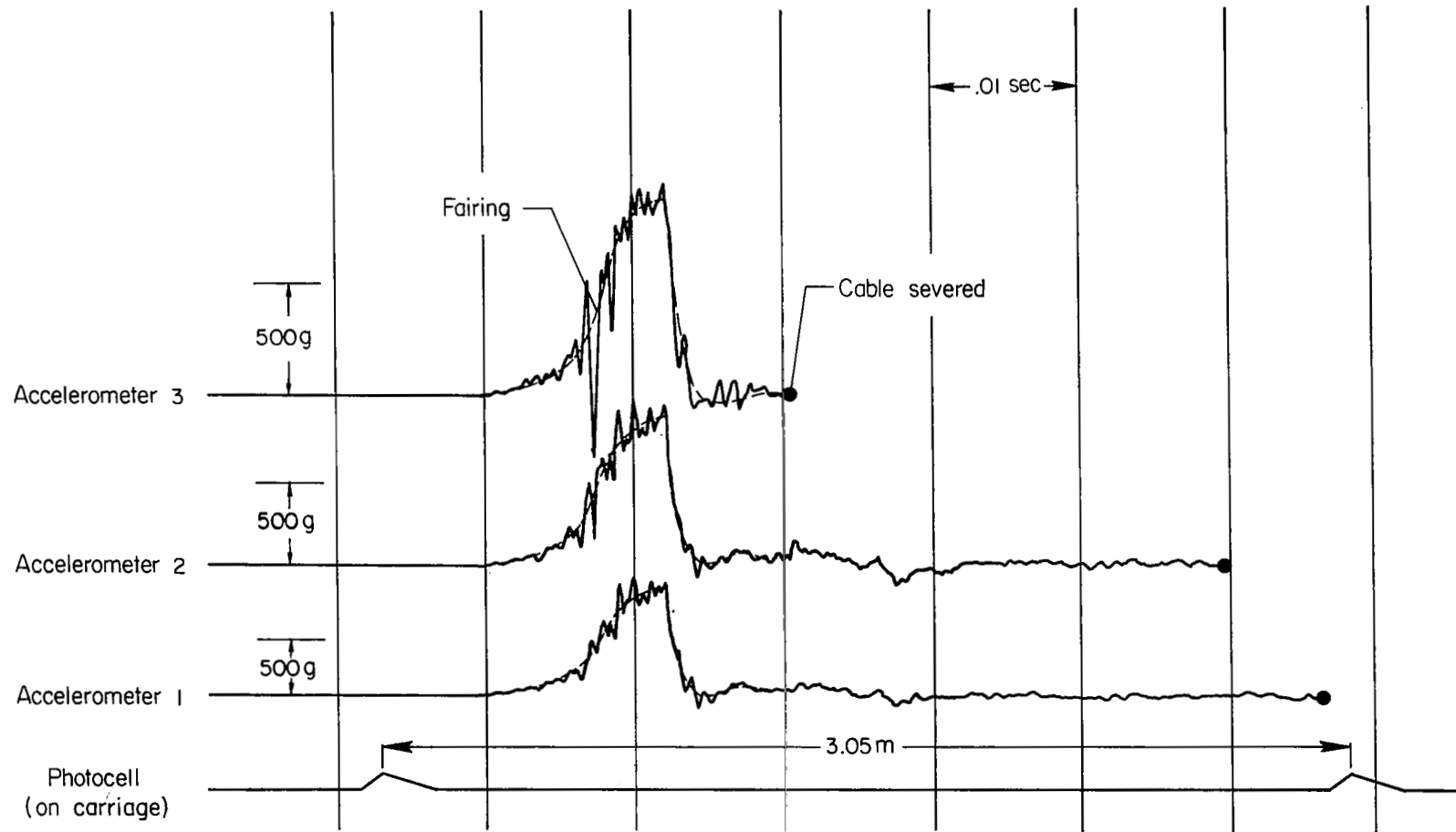


Figure 4.- Reproduction of oscillograph record showing impact acceleration time history of body 7.



$t = 0 \text{ msec}$



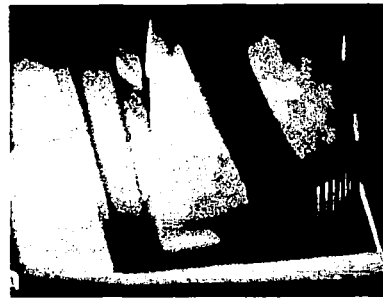
$t = 2.5 \text{ msec}$



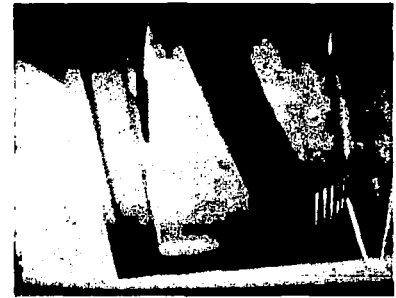
$t = 3.75 \text{ msec}$



$t = 5 \text{ msec}$



$t = 6.25 \text{ msec}$



$t = 7.5 \text{ msec}$



$t = 8.75 \text{ msec}$



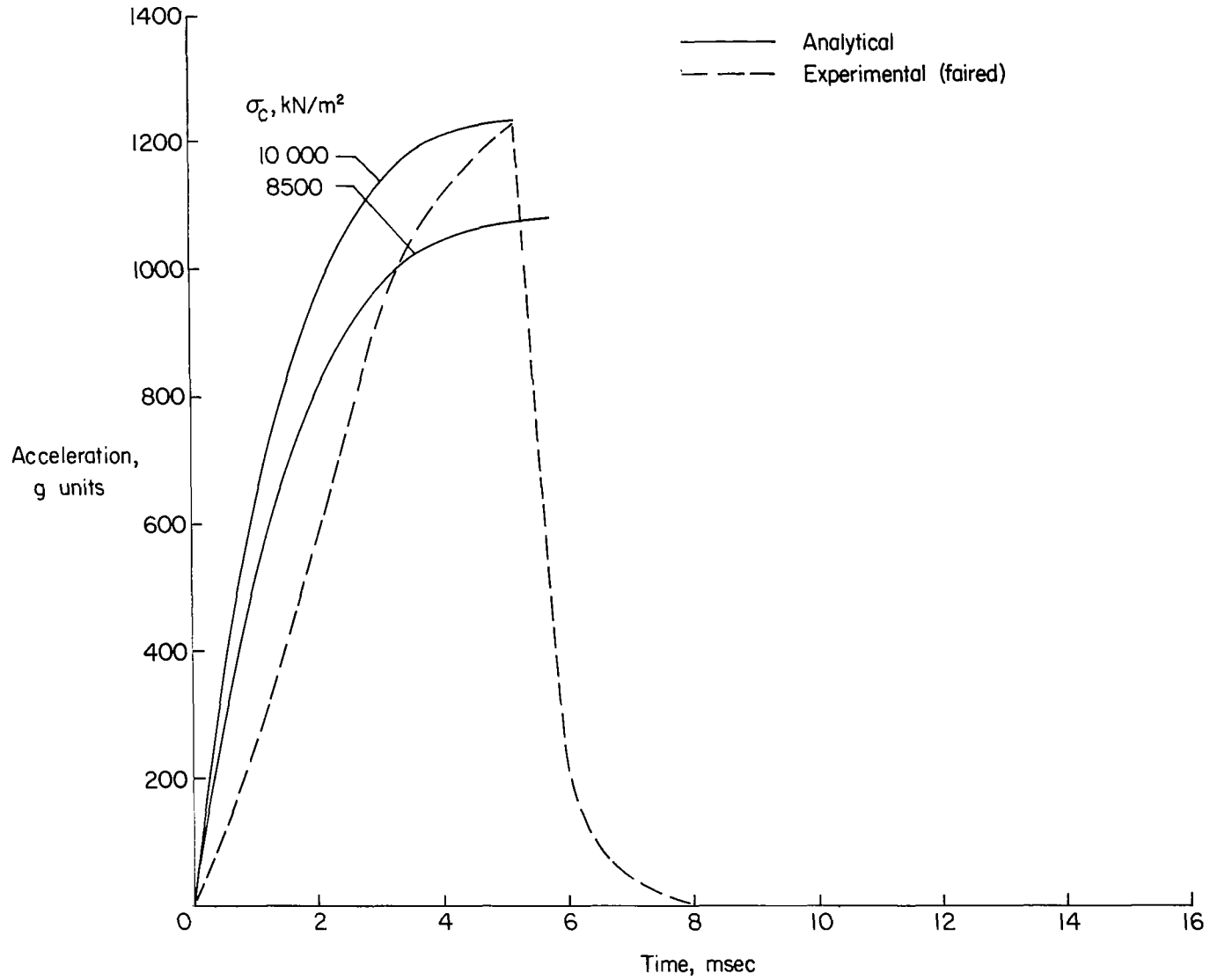
$t = 10.5 \text{ msec}$



$t = 12 \text{ msec}$

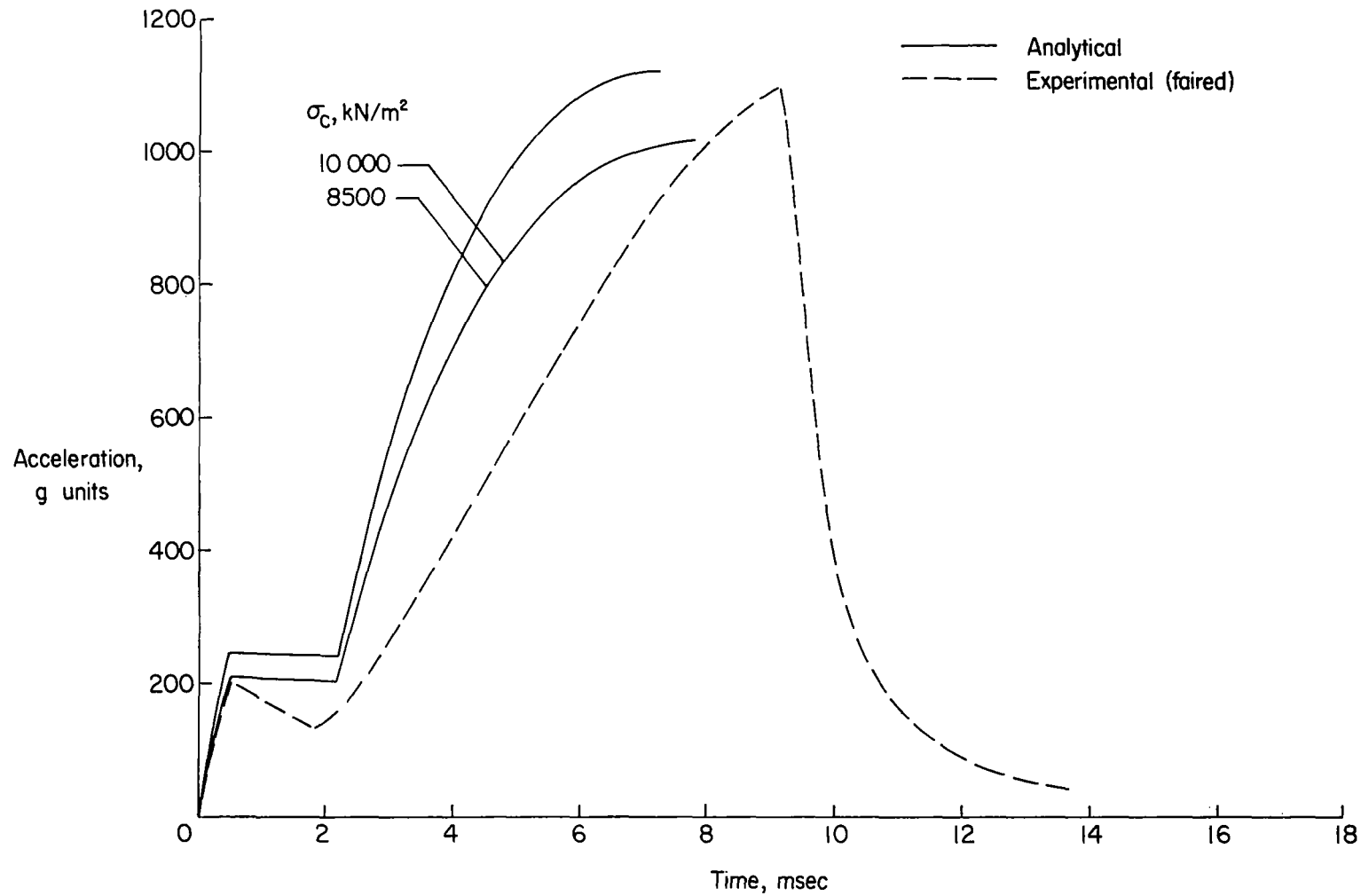
Figure 5.- Photographic sequence showing impact of body 7.

L-69-5724



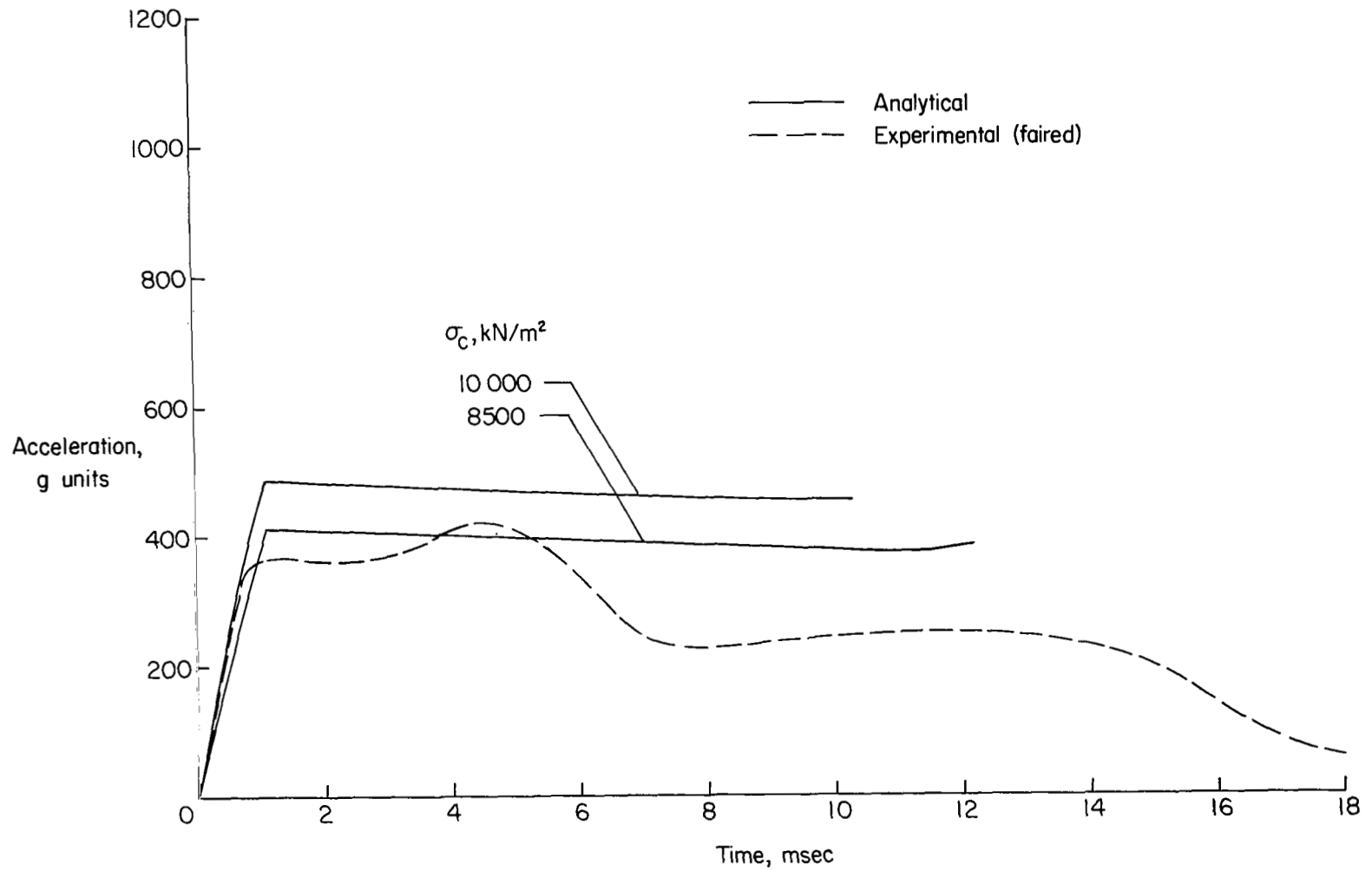
(a) Body 1 impacting flat surface; $V = 46.2$ m/sec.

Figure 6.- Analytical and experimental acceleration time histories of impacts.



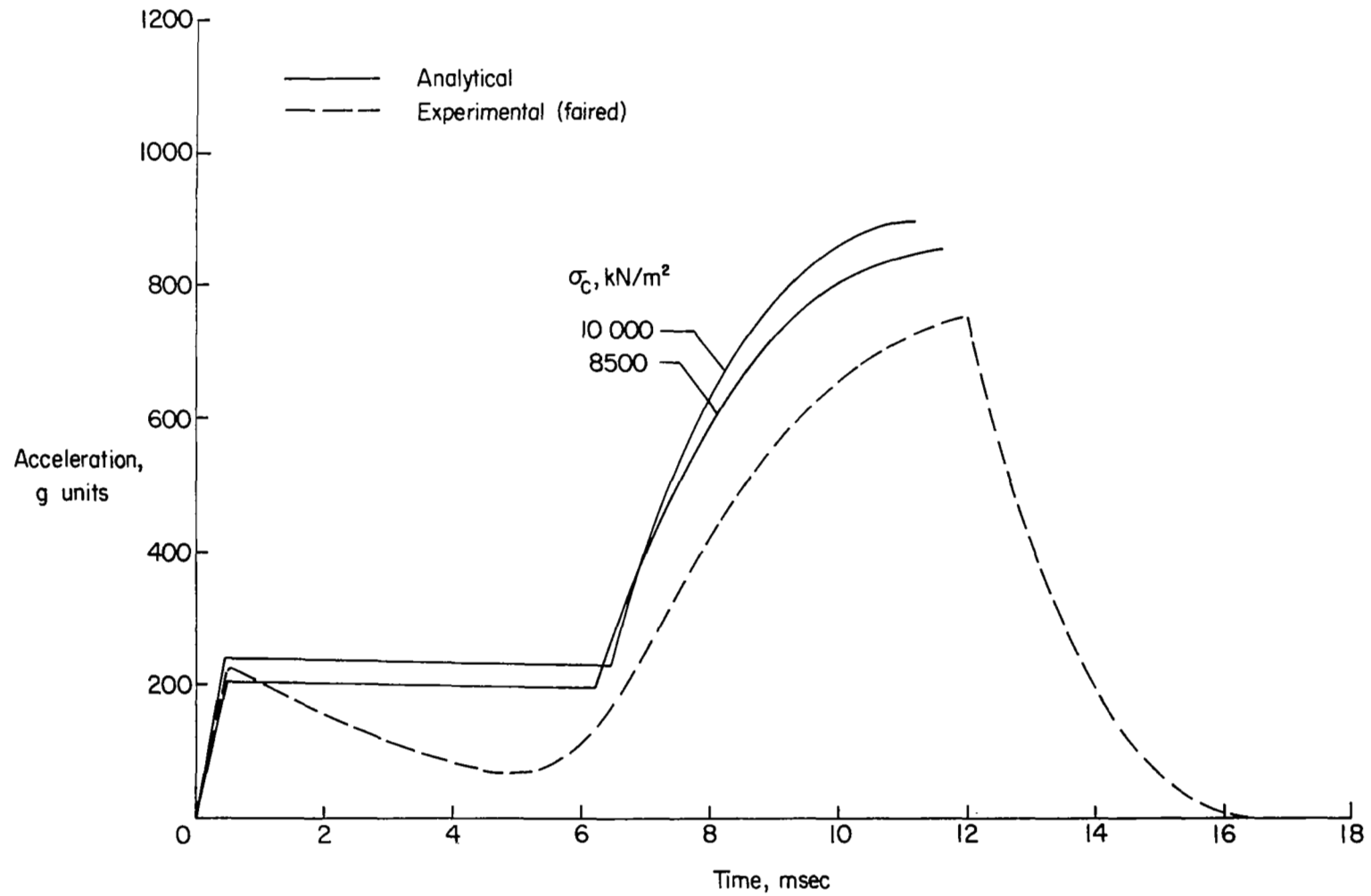
(b) Body 2 impacting cylindrical protuberance, $d_p = 38.1$ cm, $h = 7.6$ cm; $V = 47.1$ m/sec.

Figure 6.- Continued.



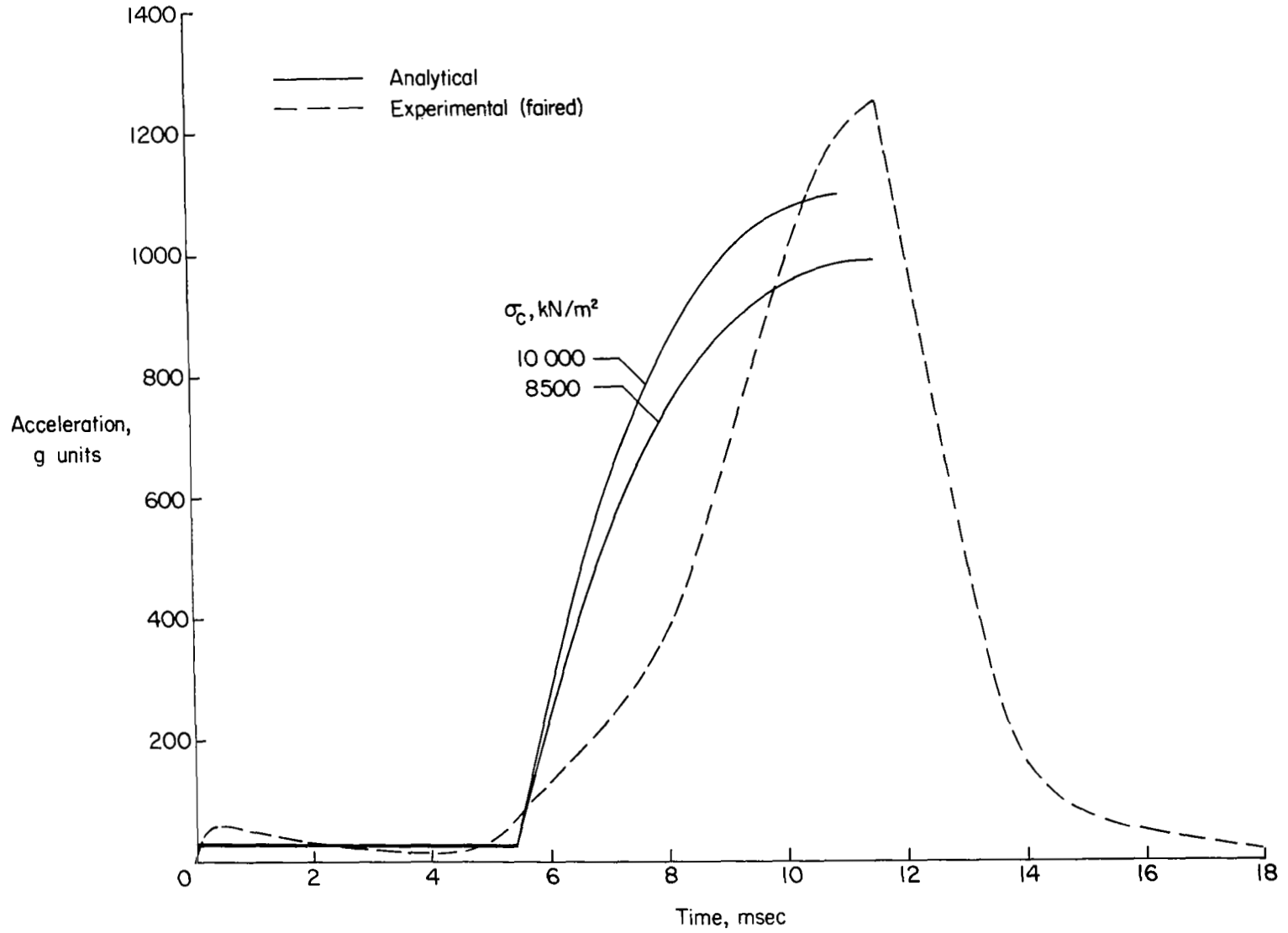
(c) Body 3 impacting cylindrical protuberance, $d_p = 55.9$ cm, $h = 22.9$ cm; $V = 44.5$ m/sec.

Figure 6.- Continued.



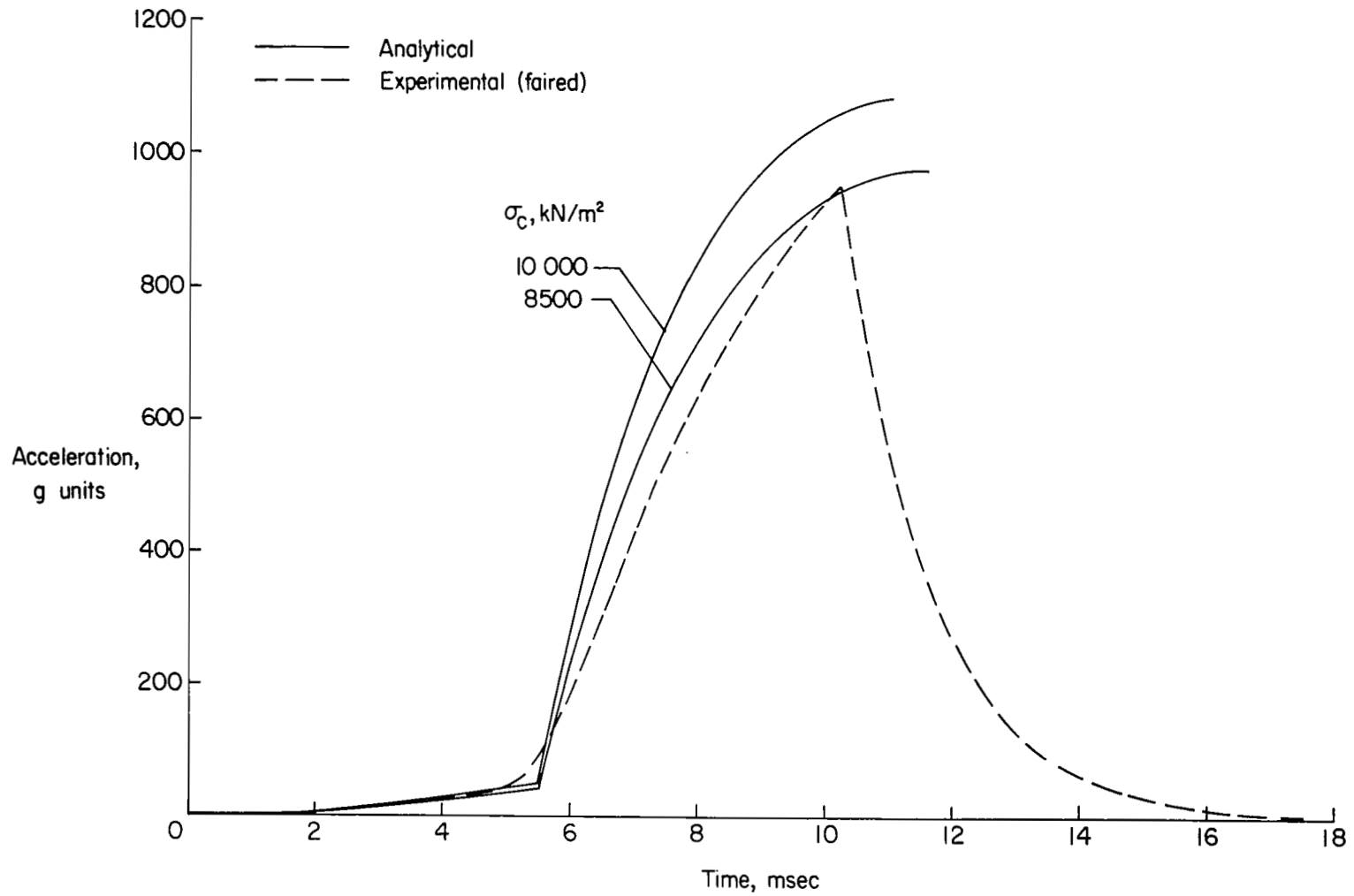
(d) Body 4 impacting cylindrical protuberance, $d_p = 38.1$ cm, $h = 22.9$ cm; $V = 45.7$ m/sec.

Figure 6.- Continued.



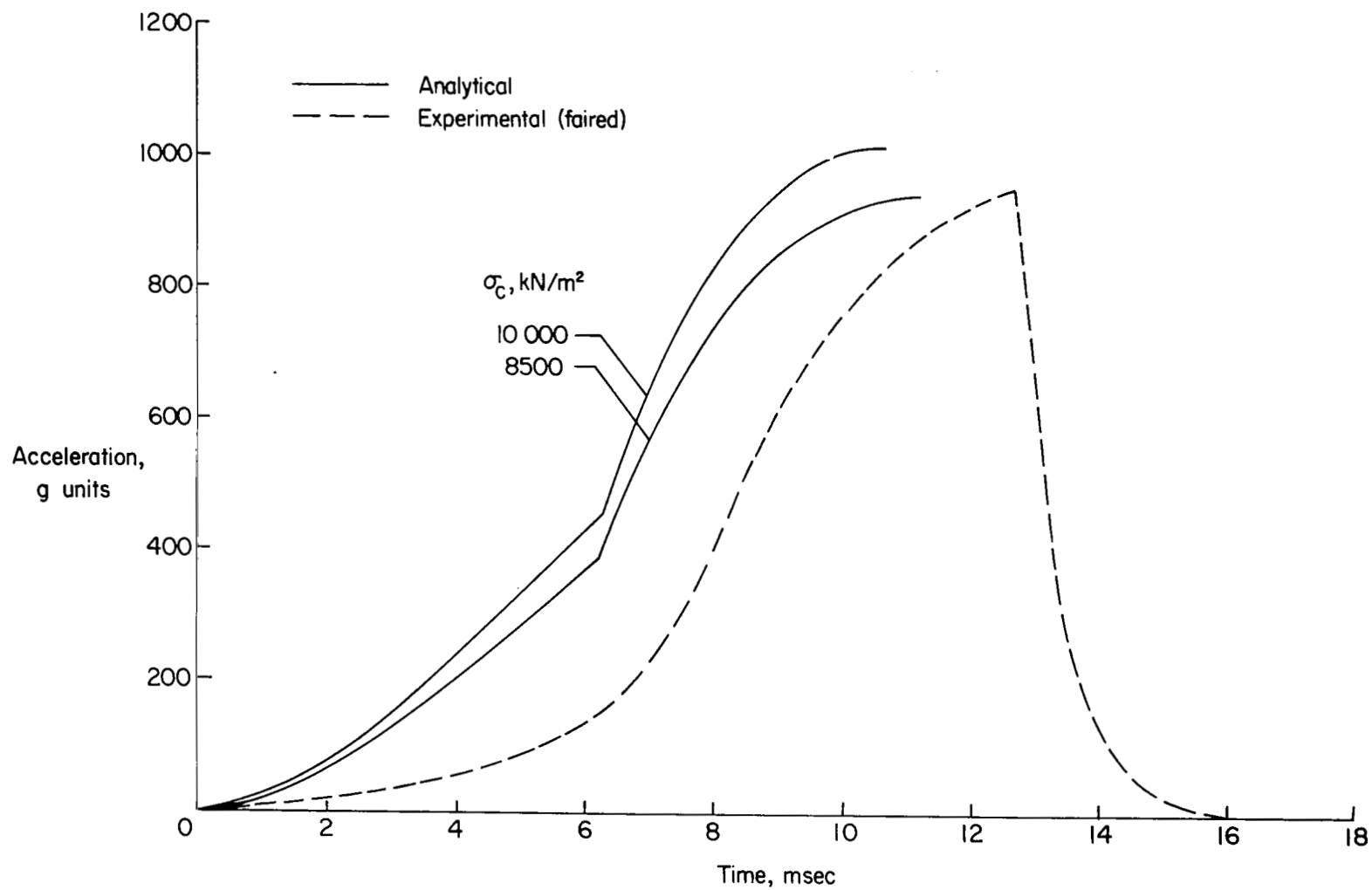
(e) Body 5 impacting cylindrical protuberance, $d_p = 12.7 \text{ cm}$, $h = 22.9 \text{ cm}$; $V = 43.2 \text{ m/sec}$.

Figure 6.- Continued.



(f) Body 6 impacting 40° conical protuberance, h = 22.9 cm; V = 42.5 m/sec.

Figure 6.- Continued.



(g) Body 7 impacting 100° conical protuberance, $h = 22.9 \text{ cm}$; $V = 46.6 \text{ m/sec}$.

Figure 6.- Concluded.

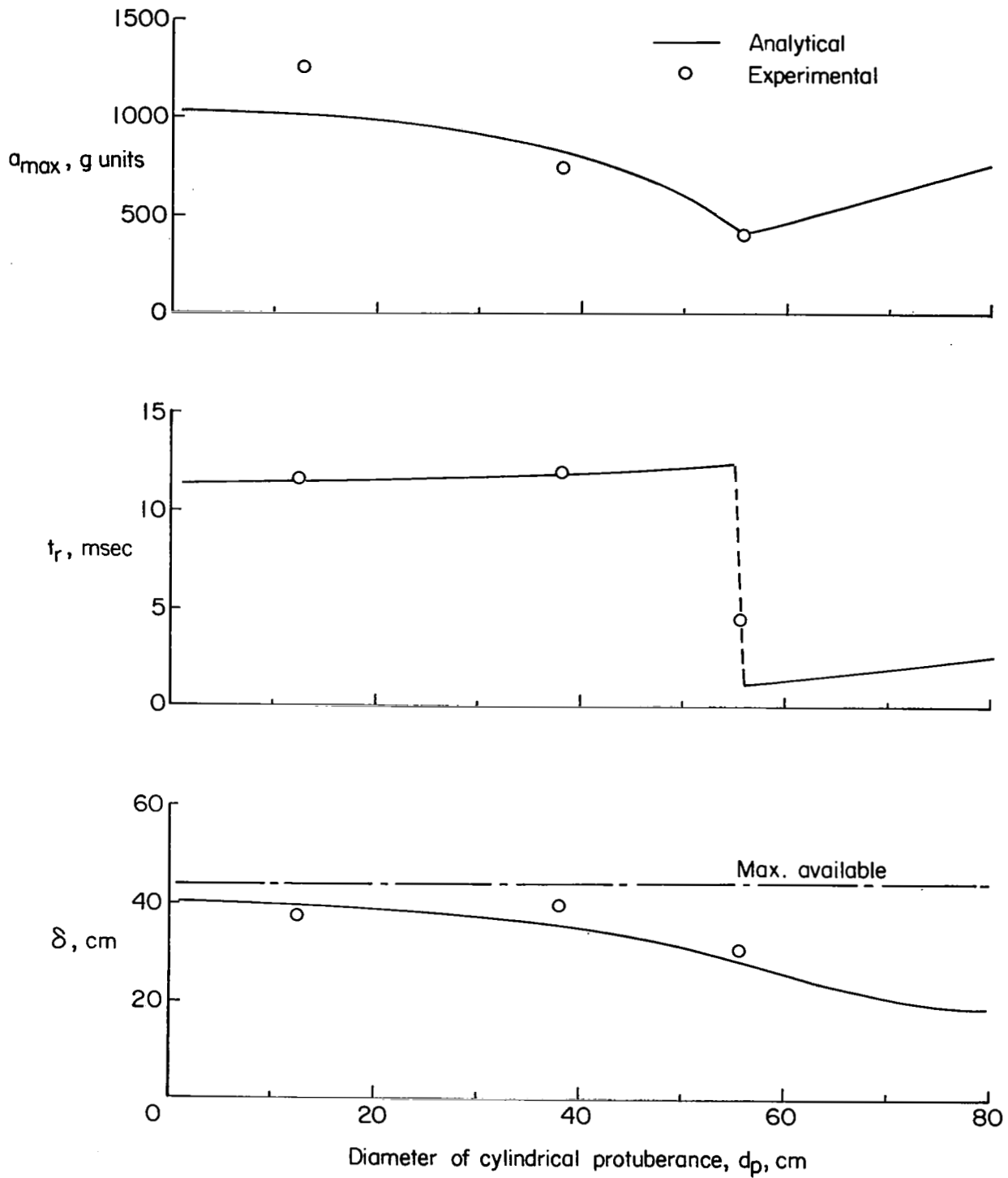


Figure 7.- Variation of significant impact characteristics with diameter of 22.9-cm-high cylindrical protuberance. For analysis, $m = 419$ kg; $\sigma_c = 8500$ kN/m²; $V = 44.5$ m/sec.

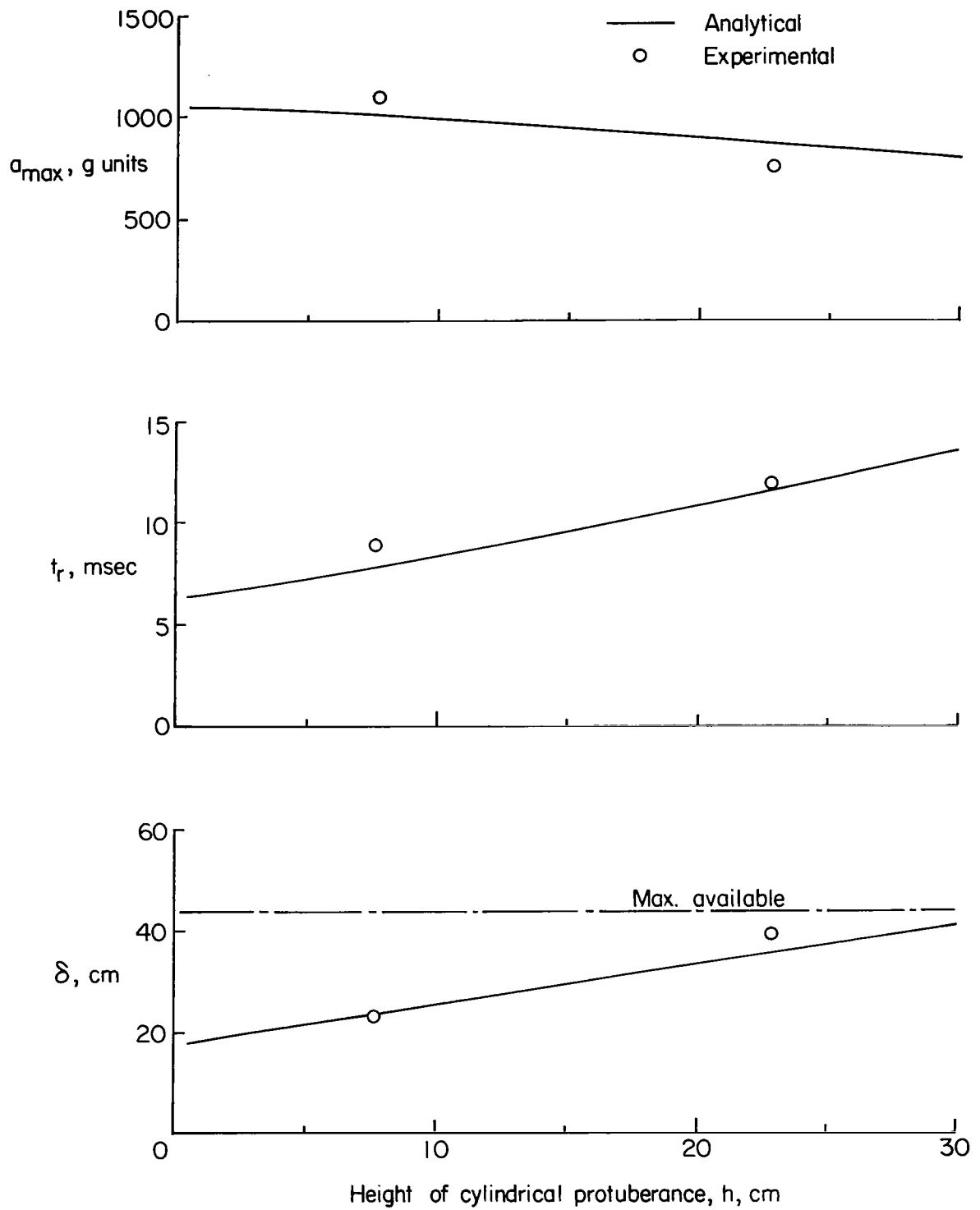


Figure 8.- Variation of significant impact characteristics with height of 38.1-cm-diameter cylindrical protuberance. For analysis, $m = 418$ kg; $\sigma_c = 8500$ kN/m²; $V = 46.4$ m/sec.

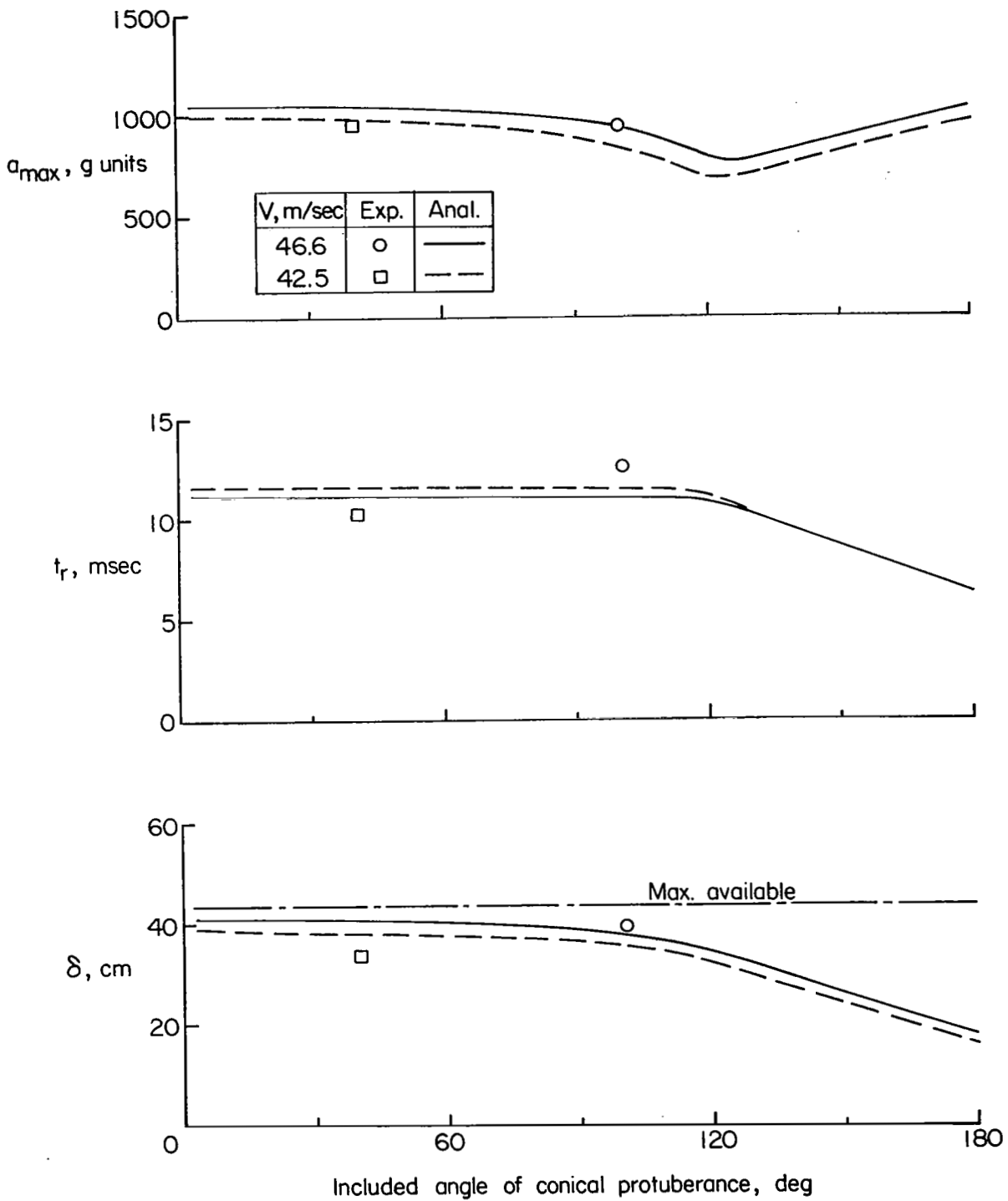


Figure 9.- Variation of significant impact characteristics with included angle of 22.9-cm-high conical protuberance. For analysis, $m = 424 \text{ kg}$; $\sigma_c = 8500 \text{ kN/m}^2$.

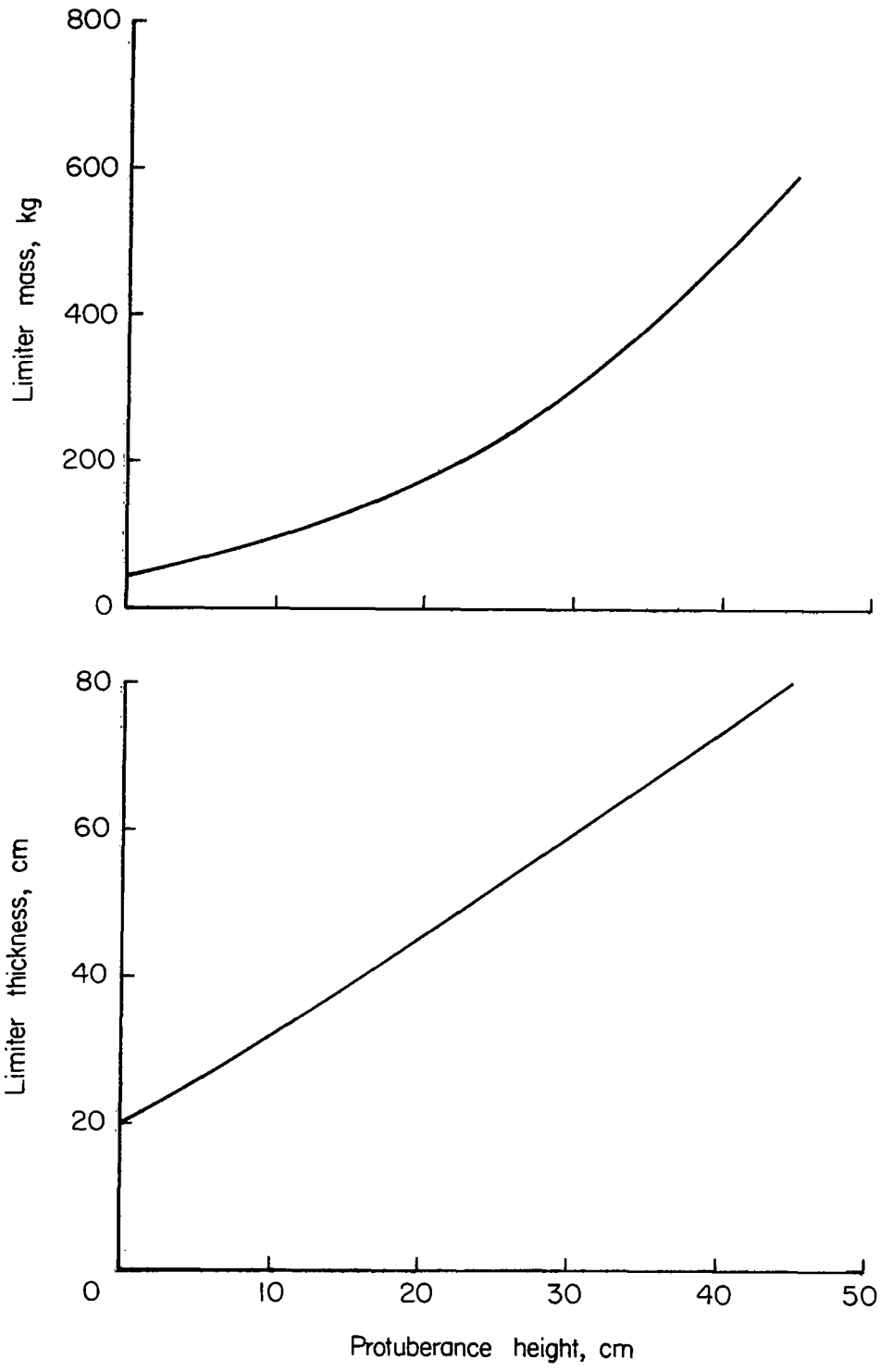


Figure 10.- Effect of protuberance height on impact limiter requirements. Payload mass, 136 kg; payload diameter, 61 cm; V = 45.7 m/sec; balsa limiter.

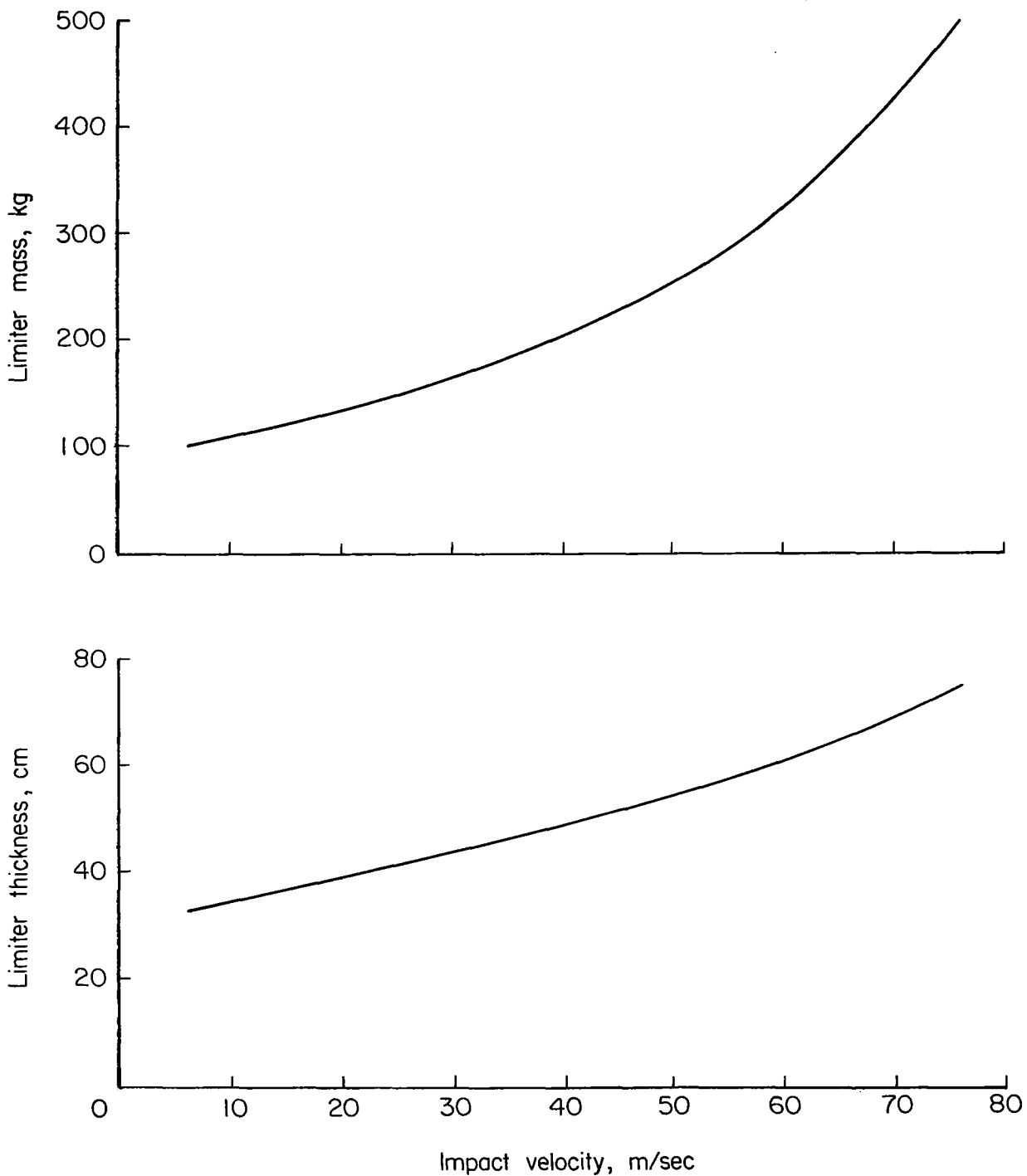


Figure 11.- Effect of velocity on impact limiter requirements for a 25-cm-high protuberance. Payload mass, 136 kg; payload diameter, 61 cm; balsa limiter.

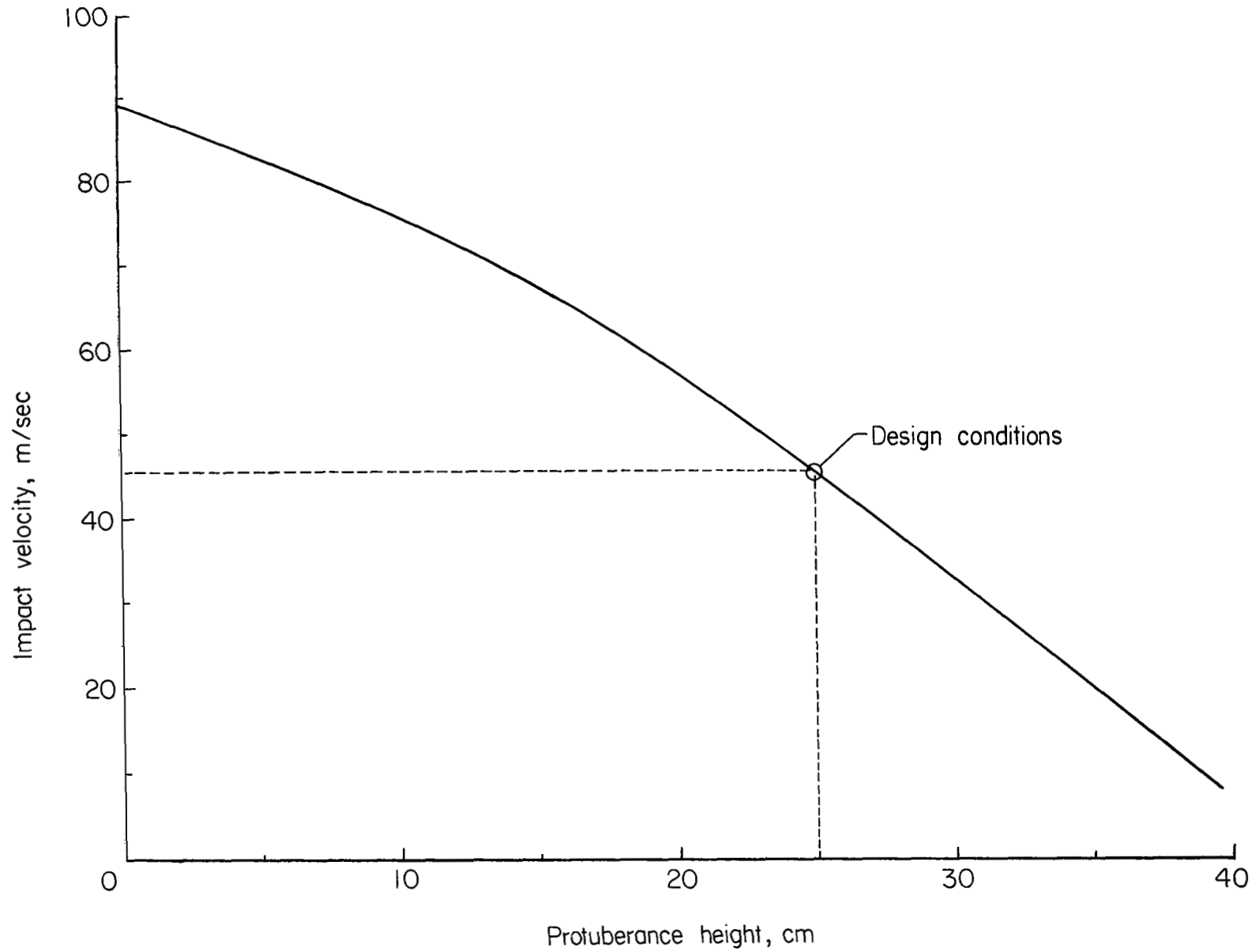


Figure 12.- Effect of protuberance height on allowable impact velocity for a fixed-configuration design. $m = 367$ kg; $d_b = 164.5$ cm; balsa limiter.

FIRST CLASS MAIL



POSTAGE AND FEES PA
NATIONAL AERONAUTICS
SPACE ADMINISTRATION

060 001 55 51 305 70043 00903
AIR FORCE WEAPONS LABORATORY /WLCL/
KIRTLAND AFB, NEW MEXICO 87117

ATTN: E. L. JOHNSON, CHIEF, TECH. LIBRARY

POSTMASTER: If Undeliverable (Section
Postal Manual) Do Not R

"The aeronautical and space activities of the United States shall be conducted so as to contribute . . . to the expansion of human knowledge of phenomena in the atmosphere and space. The Administration shall provide for the widest practicable and appropriate dissemination of information concerning its activities and the results thereof."

— NATIONAL AERONAUTICS AND SPACE ACT OF 1958

NASA SCIENTIFIC AND TECHNICAL PUBLICATIONS

TECHNICAL REPORTS: Scientific and technical information considered important, complete, and a lasting contribution to existing knowledge.

TECHNICAL NOTES: Information less broad in scope but nevertheless of importance as a contribution to existing knowledge.

TECHNICAL MEMORANDUMS: Information receiving limited distribution because of preliminary data, security classification, or other reasons.

CONTRACTOR REPORTS: Scientific and technical information generated under a NASA contract or grant and considered an important contribution to existing knowledge.

TECHNICAL TRANSLATIONS: Information published in a foreign language considered to merit NASA distribution in English.

SPECIAL PUBLICATIONS: Information derived from or of value to NASA activities. Publications include conference proceedings, monographs, data compilations, handbooks, sourcebooks, and special bibliographies.

TECHNOLOGY UTILIZATION PUBLICATIONS: Information on technology used by NASA that may be of particular interest in commercial and other non-aerospace applications. Publications include Tech Briefs, Technology Utilization Reports and Notes, and Technology Surveys.

Details on the availability of these publications may be obtained from:

**SCIENTIFIC AND TECHNICAL INFORMATION DIVISION
NATIONAL AERONAUTICS AND SPACE ADMINISTRATION
Washington, D.C. 20546**